Journal of Asian Earth Sciences 256 (2023) 105804

Contents lists available at ScienceDirect

Journal of Asian Earth Sciences

journal homepage: www.elsevier.com/locate/jseaes

Sulfide S-Zn-Cd isotopes and origin of the Liangyan Zn-Pb deposit in the Sichuan-Yunnan-Guizhou metallogenic province, SW China

Tao Wu [a], Yufan He [b], Zhiwei He [c], Zhilong Huang [a,*], Lin Ye [a], Chen Wei [d], Haifeng Fan [a], Yusi Hu [a], Lin Du [e], Minshan Gun [e]

[a] State Key Laboratory of Ore Deposit Geochemistry, Institute of Geochemistry, Chinese Academy of Sciences, Guiyang 550081, China
[b] School of Management, Guizhou University of Commerce, Guiyang 550081, China
[c] College of Earth Sciences, Chengdu University of Technology, Chengdu 610059, China
[d] Helmholtz-Zentrum Dresden-Rossendorf, Helmholtz Institute Freiberg for Resource Technology, Chemnitzer Str. 40, 09599 Freiberg, Germany
[e] Institute of Geology and Mineral Resource Exploration, Non-Ferrous Metal and Nuclear Industry Geological Exploration Bureau, Guiyang 550005, China

ARTICLE INFO

Keywords:
Zn and Cd isotopes
Metal source
Ore genesis
Mixing of isotopically distinct sources
MVT deposit

ABSTRACT

Unraveling the metal sources of Zn-Pb deposits is vital to understand the genetic types and ore-forming processes. The Sichuan-Yunnan-Guizhou metallogenic province (SYGMP) hosts abundant Zn-Pb deposits that are variably rich in critical metals such as Ga, Ge, Cd and Tl. However, sources of these critical metals and main metal Zn are still unclear. The Liangyan Cd-rich Zn-Pb deposit as a representative in the SYGMP is hosted in a carbonate sedimentary sequence and controlled by the regional Yadu-Wogong anticline and Yadu-Mangdong thrust fault. S-Zn-Cd isotopes of sulfide minerals from this deposit are obtained in order to understand the sources of metals and origin of the deposit. Sulfur isotopic results of pyrite and sphalerite reveal that sulfur was produced by thermochemical sulfate reduction (TSR) of sulfates from the Carboniferous dolostone and mudstone and the Ediacaran-Devonian carbonates. Sphalerite grains have $\delta^{66}Zn_{JMC}$ values that are negatively correlated with the $\delta^{114}Cd_{spex}$ values, implying different sources for both Zn and Cd. The variation trend of $\delta^{66}Zn_{JMC}$ and Cd/Zn suggests that Zn was mainly sourced from the Neoproterozoic basement with minor from the Carboniferous wallrocks. Besides, sphalerite grains show a negative correlation between $\delta^{114}Cd_{spex}$ and Zn/Cd, and these values fall in the field close to the Carboniferous carbonates, but away from the Permian Emeishan basalts, indicating that Cd was derived mainly from the Carboniferous wallrocks with minor from the Emeishan basalts. Together with geological evidence, the multi-isotope data suggest that the Liangyan deposit belongs to a thrust-controlled MVT Zn-Pb deposit.

1. Introduction

As an important part of the South China low-temperature metallogenic domain (LTMD), the Sichuan-Yunnan-Guizhou metallogenic province (SYGMP) in the southwestern margin of the Yangtze Block (Fig. 1a, b) was formed via the Late Indosinian (Triassic) orogenic event (Huang et al., 2011; Hu and Zhou, 2012; Hu et al., 2017, 2020; Han et al., 2022). There are over 400 Zn-Pb deposits in this province, with a total Zn and Pb resource of > 30 million tonnes (Mt), accounting for ~ 27% of the total Zn + Pb resource in China (Huang et al., 2004; Zhang et al., 2015). Regionally, these Zn-Pb deposits are strictly controlled by the Indosinian thrust and fold systems (Fig. 1c; Hu et al., 2017; Zhou et al., 2018; Wei et al., 2021; Luo et al., 2022). Many Zn-Pb deposits in this province have shown the enrichment of germanium (Ge), cadmium (Cd), gallium (Ga) and thallium (Tl), such as the Huize Ge-rich, Fule Ga-Cd-rich, and Huodehong Tl-Ge-rich Zn-Pb deposits (Huang et al., 2011; Hu et al., 2020; Hu et al., 2021; Luo et al., 2021). Previous studies of Zn-Pb deposits in the SYGMP have dealt with the field relationship, ore-material source, and mineralization age (Zhang et al., 2015; Yang et al., 2019; Luo et al., 2020). However, understanding of metal sources and origin of these deposits is still poor. For instance, the sources of Zn and Pb have been variably attributed to Neoproterozoic metamorphic

* Corresponding author.
E-mail addresses: wutao@mail.gyig.ac.cn (T. Wu), beliefhyf@foxmail.com (Y. He), 414589747@qq.com (Z. He), huangzhilong@vip.gyig.ac.cn (Z. Huang), yelin@vip.gyig.ac.cn (L. Ye), weichen@mail.gyig.ac.cn (C. Wei), fanhaifeng@mail.gyig.ac.cn (F. Haifeng), huyusi@mail.gyig.ac.cn (Y. Hu), 370611046@qq.com (L. Du), GunMinshan123@163.com (M. Gun).

https://doi.org/10.1016/j.jseaes.2023.105804
Received 17 April 2023; Received in revised form 19 July 2023; Accepted 26 July 2023
Available online 27 July 2023

basement complexes, Ediacaran-Permian ore-hosting wallrocks, and/or Permian Emeishan basalts (e.g. Wu et al., 2021b and references therein).

The Liangyan Zn-Pb deposit in the southeastern part of the SYGMP has the reserves of ~ 40000 t Zn + Pb and ~ 120 t Cd (Liao et al., 2020). This deposit is hosted in Carboniferous dolostone/limestone and structurally controlled by the Yadu-Mangdong thrust fault and Yadu-Wogong anticline (Fig. 2; Wan, 2015; Zhou, 2017). The Zn-Pb orebodies together with the Carboniferous hosting carbonates were thrusted over the Emeishan basalts along the regional Yadu-Mangdong fault (Fig. 3). The Liangyan deposit is ideal for studying the Zn-Pb mineralization in the SYGMP. Although detailed studies of this deposit are available in literature (Wan, 2015; Zhou, 2017; Wang et al., 2019; Liao et al., 2020; Han

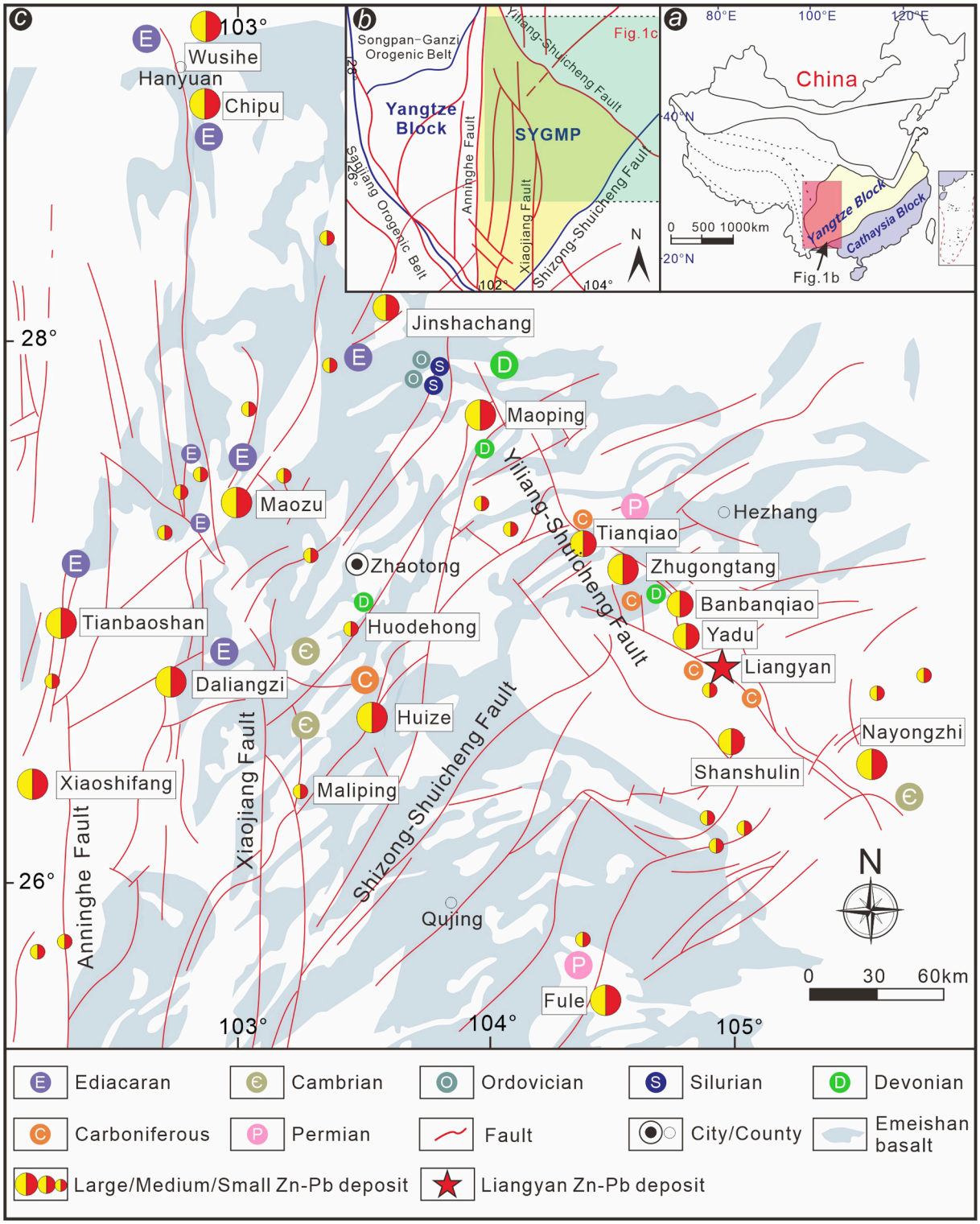

Fig. 1. (a) Tectonic map of China, showing the locations of the Yangtze Block and the Sichuan-Yunnan-Guizhou metallogenic province (SYGMP) (modified after Wu et al., 2021b); (b) Geotectonic map (modified after Wei et al., 2021) and (c) regional geologic map of the SYGMP, showing the distribution of sedimentary sequences, Emeishan basalts, major structures, and Zn-Pb deposits (modified after Liu and Lin, 1999).

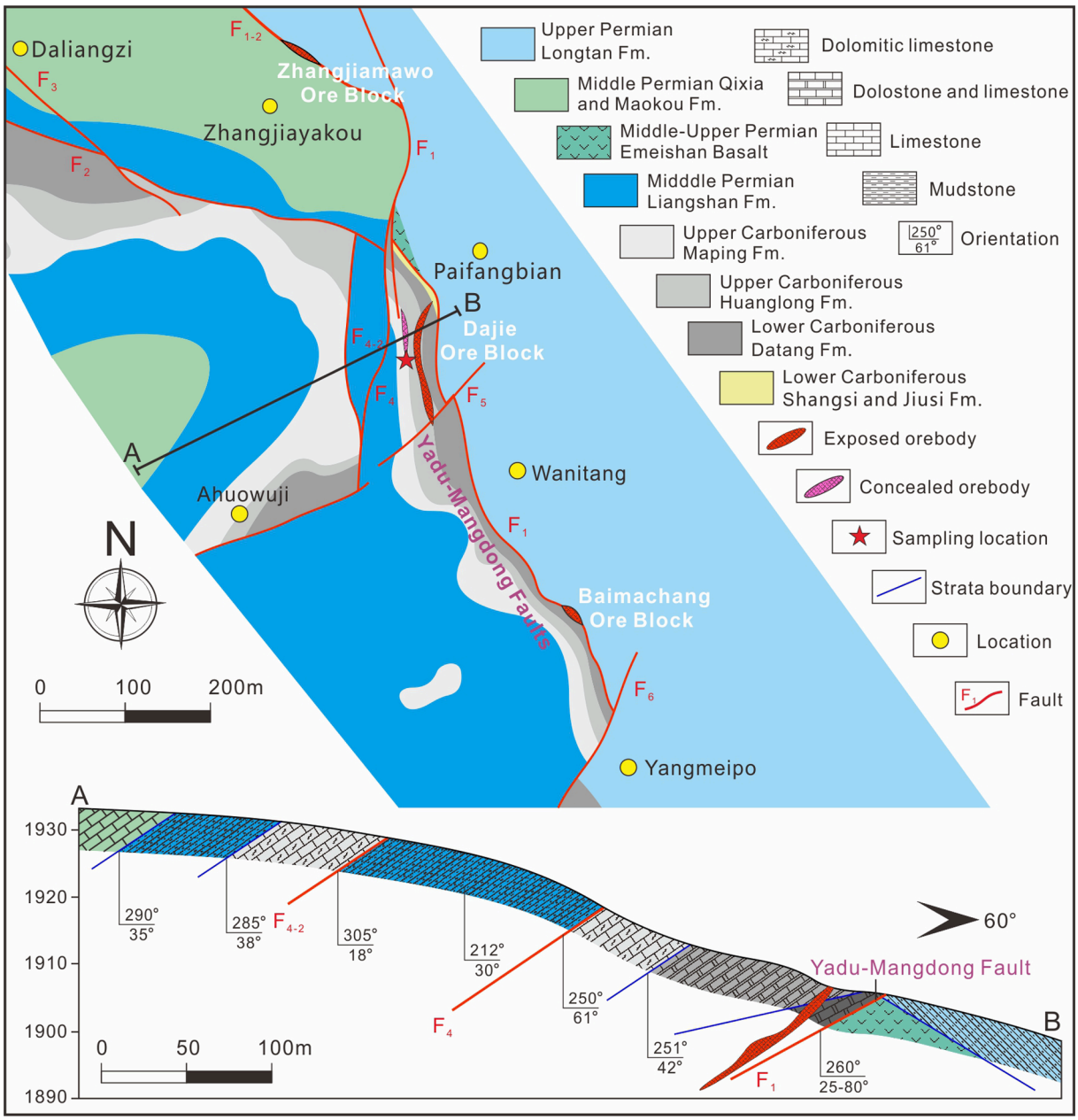

Fig. 2. Geological sketch map of the Liangyan Zn-Pb deposit, showing sedimentary sequences, faults, orebodies, and the geological profile A-B (modified from Wan, 2015; Zhou, 2017).

et al., 2022), sources of S and metals Zn and Cd are still poorly understood.

Studies of stable Zn and Cd isotopes using multi-collector inductively coupled plasma mass spectrometer (MC-ICP-MS) have significantly advanced our knowledge about sources of ore metals and thus origin of Zn-Pb deposits (Wombacher et al., 2003; Wilkinson et al., 2005; Kelley et al., 2009; Zhu et al., 2013, 2017, 2021; Zhou et al., 2014a; Wen et al., 2016; Xu et al., 2019; Wu et al., 2021b). In this contribution, S isotopes of pyrite and sphalerite and Zn and Cd isotopes of sphalerite from the Liangyan deposit are integrated to trace the sources of S, Zn, and Cd and to provide constraints on the origin of the deposit. Our findings yield new insights about the origin of the carbonate-hosted Zn-Pb deposits along thrust-fold belts in the SYGMP.

2. Geological background

2.1. Regional geology

South China is geologically composed of the Yangtze Block to the NW and Cathaysia Block to the SE (Fig. 1a), and has undergone multistage tectono-thermal events since the Neoproterozoic (Wang et al., 2013; Shu et al., 2015; Hu et al., 2017). The South China low temperature metallogenic domain (LTMD) in the Yangtze Block includes the SYGMP, Xiangzhong Sb-Au and Youjiang Au-As-Sb-Hg metallogenic provinces. The SYGMP is bounded by the NE-trending Shizong-Shuicheng, NS-trending Anninghe, and the NW-trending Yiliang-Shuicheng regional faults (Huang et al., 2004; Hu et al., 2017; Ren et al., 2018; Wei et al., 2018; Fig. 1b). The regional basement is composed of Paleoproterozoic metamorphic complexes, Mesoproterozoic Dongchuan Group *meta-*

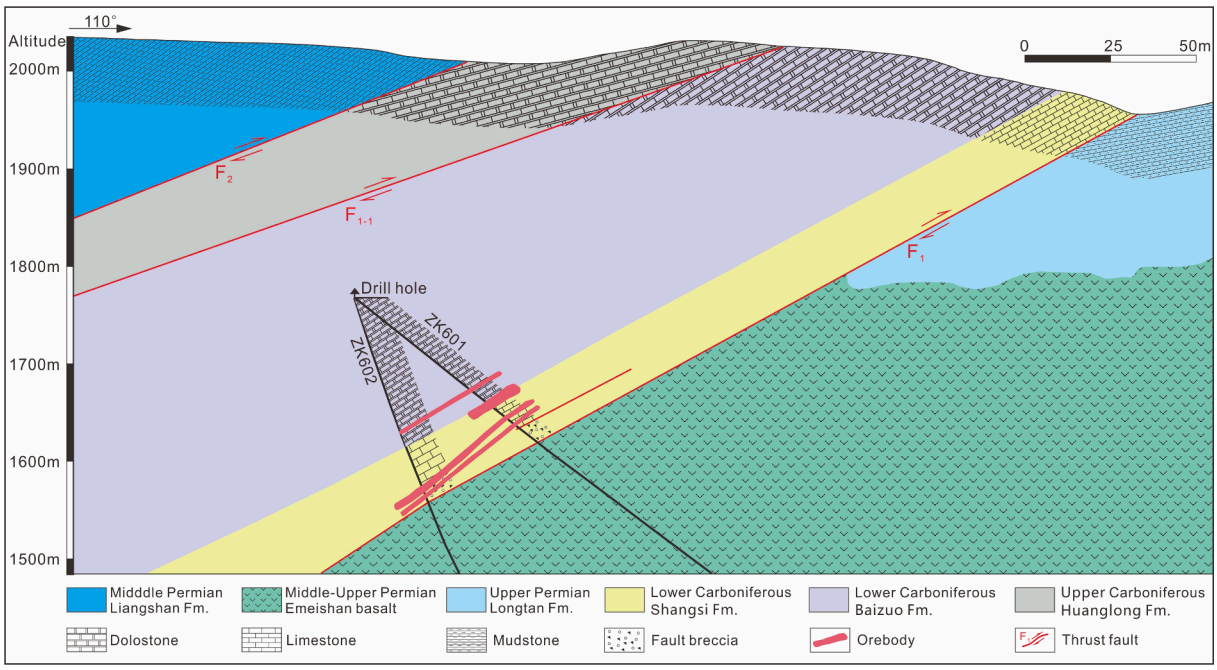

Fig. 3. Geological profile No. 6 in the Liangyan deposit, showing the different stratigraphic units, thrust faults, and some orebodies (modified after Liao et al., 2020).

clastic and volcanic-sedimentary rocks, and Neoproterozoic Huili and Kunyang Groups metamorphic clastic and carbonate rocks (Yan et al., 2003; Wang et al., 2019; Luo et al., 2022). The overlying sedimentary sequences comprise mainly the Ediacaran-Triassic marine carbonates, which are overlaid by the Jurassic terrestrial clastic/argillaceous sedimentary rocks (Liu and Lin, 1999; Wang et al., 2019; He et al., 2020). The mantle-plume related ~ 260 Ma Emeishan continental flood basalts are widespread in the region, and are spatially associated with the Zn-Pb mineralization (Fig. 1c; Huang et al., 2004; Li et al., 2004; Hu and Zhou, 2012; Zhang et al., 2015; Hu et al., 2017).

2.2. Deposit geology

In the intersection of the NW-trending Yadu-Mangdong thrust fault and Yadu-Wogong anticline, the Liangyan carbonate-hosted Zn-Pb district is composed of the Carboniferous to Permian sedimentary carbonate and clastic rocks (Fig. 2; Zhou, 2017; Wang et al., 2019). The Carboniferous Shangsi, Baizuo, Datang, and Huanglong Formations host the main Zn-Pb orebodies and are mainly composed of dolostone, limestone and bioclastic/dolomitic limestone (Figs. 2 and 3; Wan, 2015; Zhou, 2017). The overlying Permian sequence includes mainly: (i) Middle Permian Liangshan Fm. mudstone, sandstone, and argillaceous siltstone, (ii) Middle Permian Maokou Fm. bioclastic/dolomitic limestone, (iii) Middle-Upper Permian Emeishan Fm. continental flood basalts (unconformable contact with overlying Maokou Formation and underlying Longtan Formation), and (iv) Upper Permian Longtan Fm. mudstone, sandstone, and shale (Figs. 2 and 3; Wan, 2015; Zhou, 2017).

In the Liangyan ore district, NW-, NE-, and NS-trending faults are well developed (Figs. 2 and 3). The NW-trending Yadu-Mangdong thrust fault (F_1) and its secondary faults ($F_{1\text{-}1}$, $F_{1\text{-}2}$, F_2, and F_3), 2–4 km along strike (dipping 55°–80°), were interpreted as ore-fluid conduits and Zn-Pb ore precipitation sites (Zhou, 2017). The F_1 thrust fault with throw>1 km caused the Carboniferous ore-hosting strata to thrust partially over the Permian Emeishan basalts (Fig. 3). Besides, the NS-trending thrust faults (F_4 and $F_{4\text{-}2}$) are ~ 2 km long with a dip of 52°–65°, which locally merged with F_1 in the northeastern of the ore district (Fig. 2). The small dextral strike-slip faults (F_5 and F_6) are ~ 0.5 km long and trends 30°–40° (dip angle: 35°–60°), which cut the main ore-hosting F_1 fault (Fig. 2; Wan, 2015; Zhou, 2017).

The Liangyan deposit is composed of three main ore blocks, i.e., Zhoujiamawo, Dajie and Baimachang from north to south (Fig. 2). Zn-Pb orebodies are hosted in the Carboniferous carbonate rocks along the Yadu-Mangdong thrust fault and its secondary structures and occur as stratiform, veined, or lenticular bodies (Figs. 2 and 3). Orebodies at Zhoujiamawo are hosted in the dolomitic limestone and are 80–100 m long, 60 m wide, 1.2–1.5 m thick. Ores contain 3–7% Zn and 2–3% Pb. Orebodies at Dajie are hosted in dolostone and limestone, accounting for 80% of the total metal reserve in the Liangyan deposit, and are 13–105 m long, 26–298 m wide, 1.0–8.7 m thick. Ores contain 5.7% Zn and 1.4% Pb. Orebodies at Bamachang are hosted in the dolostone and are 80 m long, 100 m wide, 2.0 m thick, with an ore grade of 2–6% Zn and 2–5% Pb. The Zn-Pb ores are mainly sulfides and minor oxides. The sulfides ores are characterized by open-space filling and carbonate-replacement types, with massive (Fig. 4a, e and g), disseminated (Fig. 4c and f), or veined (Fig. 4b, d and h) textures. Metallic minerals include mainly sphalerite, pyrite, and galena, whilst non-metallic minerals include mainly calcite and dolomite (Fig. 4). The metallic minerals are euhedral to anhedral, and have granular (Fig. 4i-j, l-o), replacement (Fig. 4i-j, n-o), crosscutting vein (Fig. 4k, p and l), and inclusion (Fig. 4m and o) textures.

3. Sampling and analytical methods

3.1. Sampling

In this study, sulfide ore samples were collected from the 1650 m, 1723 m and 1770 m adits of the Dajie ore block. Sulfide (sphalerite and pyrite) separates were handpicked from the crushed sulfide ore samples under a binocular microscope. Representative ore-stage pyrite (n = 7) and reddish/yellowish-brown sphalerite (n = 15) were selected for the S-Zn-Cd isotopic analyses. Petrographic characteristics and sampling location of these samples were shown in Fig. 2 and Tables 1 and 2.

3.2. Sulfur isotope analysis

The $\delta^{34}S$ isotope analyses of pyrite and sphalerite from the Liangyan deposit were carried out at the State Key Laboratory of Ore Deposit Geochemistry (SKLODG), Institute of Geochemistry, Chinese Academy

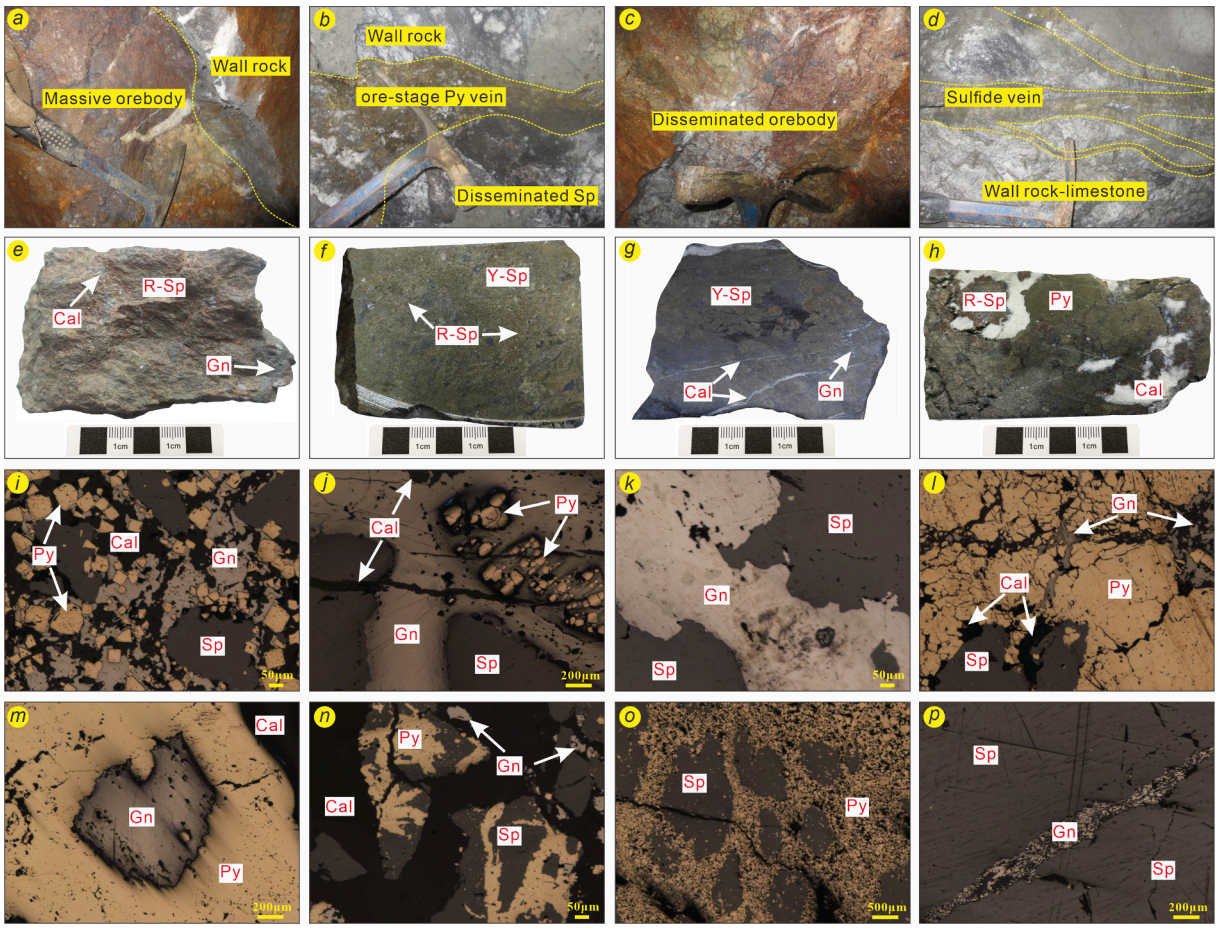

Fig. 4. Field (a-d), hand-specimen (e-h), and microscope (i-p) photographs of the occurrence and textures of sulfide orebodies and ores in the Liangyan deposit: (a) Contact between massive orebody and carbonate wallrocks; (b) Disseminated sphalerite replaced by late ore-stage pyrite; (c) Disseminated sulfide orebody; (d) Carbonate wallrocks infilled by sulfide vein; (e) Reddish-brown sphalerite replaced by galena; (f) veined reddish-brown sphalerite replaced by massive yellowish-brown sphalerite; (g) Massive sulfide ore, showing coarse-grained yellowish-brown sphalerite replaced by late galena and calcite; (h) Reddish-brown sphalerite enclosed by calcite and cut the early pyrite; (i) Euhedral-subhedral pyrite replaced by late sphalerite and galena; (j) Subhedral-anhedral pyrite enclosed by coarse-grained sphalerite and galena; (k) Symbiotic sphalerite and galena; (l) Pyrite and sphalerite cut by late galena and calcite; (m) Anhedral galena enclosed by coarse-grained pyrite; (n) Anhedral sphalerite replaced by late pyrite and galena; (o) Anhedral sphalerite replaced by porous pyrite; (p) Coarse-grained sphalerite cut by galena vein. Abbreviations: Gn: galena; R-Sp: reddish-brown sphalerite; Y-Sp: yellowish-brown sphalerite; Py: pyrite; Cal: calcite.

Table 1
Sulfur isotope compositions of sulfides from the Liangyan deposit.

Sample no.	Mineral	Location	$\delta^{34}S$/‰	Sample no.	Mineral	Location	$\delta^{34}S$/‰
1LY-3	Pyrite	1650 m adit	+23.09	LY-12	Reddish-brown sphalerite	1650 m adit	+22.59
1LY-5	Pyrite	1650 m adit	+22.70	LY-25–1	Yellowish-brown sphalerite	1723 m adit	+20.98
1LY-6	Pyrite	1650 m adit	+22.81	LY-25–2	Reddish-brown sphalerite	1723 m adit	+22.10
1LY-9	Pyrite	1650 m adit	+22.14	LY-25–5	Reddish-brown sphalerite	1723 m adit	+22.35
LY-13	Pyrite	1650 m adit	+23.48	LY-10①	Reddish-brown sphalerite	1723 m adit	+21.18
LY-14	Pyrite	1650 m adit	+23.48	LY-10②	Yellowish-brown sphalerite	1723 m adit	+21.34
LY-16	Pyrite	1650 m adit	+22.40	LY-24–1	Reddish-brown sphalerite	1770 m adit	+22.03
1LY-1	Yellowish-brown sphalerite	1650 m adit	+21.80	LY-24-3①	Yellowish-brown sphalerite	1770 m adit	+20.50
1LY-4①	Reddish-brown sphalerite	1650 m adit	+21.98	LY-24-3②	Reddish-brown sphalerite	1770 m adit	+22.30
1LY-4②	Yellowish-brown sphalerite	1650 m adit	+20.80	LY-24-4①	Yellowish-brown sphalerite	1770 m adit	+22.35
1LY-7	Yellowish-brown sphalerite	1650 m adit	+20.78	LY-24-4②	Reddish-brown sphalerite	1770 m adit	+23.21

of Sciences (IGCAS), using a Finnigan MAT-253 mass spectrometer. The $\delta^{34}S$ value was determined on SO_2, which was liberated from sulfide-Cu_2O composite under vacuum system under given P-T conditions. IAEA S-1 (-0.2‰), IAEA S-2 (+22.6‰), and IAEA S-3 (–32.5‰) were used as the external standards. The $\delta^{34}S$ value was reported relative to the Vienna Canyon Diablo Troilite (V-CDT), with analytical precision better than ± 0.2‰.

3.3. Zn and Cd isotope analyses

The digestion of sphalerite grains, chemical separation and purification of Zn and Cd, and measurement of Zn-Cd isotopes were conducted at the SKLODG, IGCAS. Specific extraction procedures were as described by Tang et al. (2006) and Zhu et al. (2016). The Zn-Cd isotope compositions were measured on a Thermo Fisher Scientific Neptune Plus multi-collector inductively coupled plasma mass spectrometer (MC-ICP-MS),

Table 2
Zn-Cd isotope compositions of sphalerite and potential source rocks in the Liangyan deposit.

Sample no.	Object	Position	$\delta^{114}Cd_{spex}$/‰	2SD	$\delta^{66}Zn_{JMC}$/‰	2SD	Cd (ppm)	Zn/%	Zn/Cd	Cd/Zn	Source
1LY-1	Yellowish-brown Sp	1650 *m*	+0.05	0.01	+0.55	0.01	6885	46.0	66.8	0.015	This paper
1LY-4①	Reddish-brown Sp	1650 *m*	−0.11	0.03	+0.44	0.01	6721	62.2	92.6	0.011	
1LY-4②	Yellowish-brown Sp	1650 *m*	−0.05	0.03	+0.48	0.06	5803	55.3	95.3	0.010	
1LY-7	Yellowish-brown Sp	1650 *m*	−0.12	0.06	+0.48	0.02	6880	51.0	74.1	0.013	
LY-12	Reddish-brown Sp	1650 *m*	+0.14	0.00	+0.28	0.01	14,250	42.5	29.8	0.034	
LY-10①	Reddish-brown Sp	1723 *m*	−0.04	0.07	+0.48	0.01	9344	53.1	56.8	0.018	
LY-10②	Yellowish-brown Sp	1723 *m*	−0.01	0.02	+0.48	0.05	8852	58.4	65.9	0.015	
LY-25–1	Yellowish-brown Sp	1723 *m*	+0.25	0.01	+0.37	0.03	8667	50.8	58.6	0.017	
LY-25–2	Reddish-brown Sp	1723 *m*	+0.39	0			9000	64.5	71.7	0.014	
LY-25–5	Reddish-brown Sp	1723 *m*	+0.2	0.10	+0.47	0.05	7000	42.7	61.0	0.016	
LY-24–1	Reddish-brown Sp	1770 *m*	+0.01	0.01			11,475	49.5	43.1	0.023	
LY-24-3①	Yellowish-brown Sp	1770 *m*	+0.04	0.02			8951	54.6	61.0	0.016	
LY-24-3②	Reddish-brown Sp	1770 *m*	+0.07	0.07	+0.42	0.02	11,803	46.0	38.9	0.026	
LY-24-4①	Yellowish-brown Sp	1770 *m*	+0.19	0.03	+0.47	0.01	17,333	52.8	30.5	0.033	
LY-24-4②	Reddish-brown Sp	1770 *m*	+0.33	0.08	+0.40	0.04	17,333	43.6	25.2	0.040	
HZ-16	Limestone	Carboniferous	+0.08	0.04			0.68	$15*10^{-4}$	22.0	0.045	Zhu et al. 2021
HZ-17	Limestone	Maping Fm.	+0.17	0.12			0.70	$18*10^{-4}$	26.0	0.039	
HZ-14	Dolomite	Carboniferous	+0.20	0.04	+0.15	0.04	0.35	$26*10^{-4}$	74.0	0.013	
HZ-22	Dolomite	Baizuo Fm.	+0.13	0.10	+0.17	0.05	0.81	$47*10^{-4}$	58.0	0.017	
HZ-08	Limestone	Carboniferous	+0.00	0.01	−0.12	0.04	0.29	$30*10^{-4}$	103	0.010	
HZ-12	Limestone	Datang Fm.	+0.42	0.03			0.13	$10*10^{-4}$	77.0	0.013	
HZ-13	Limestone		+0.15	0.06			0.46	$19*10^{-4}$	41.0	0.024	
HZ-11–1	Basalt	Permian	−0.14	0.01			0.18	$136*10^{-4}$	756		Zhu et al. 2017
HZ-11–1	Basalt		−0.13	0.01			0.18	$136*10^{-4}$	756		
HZ-11–2	Basalt		−0.22	0.04			0.11	$99*10^{-4}$	900		
TBS16-2	Graywacke	Kunyang			+0.30	0.03	0.02	$86*10^{-4}$		0.000	Zhu, 2014;
WC-1	Dolostone	and Huili Gp.			+0.21	0.04	0.04	4*10–4		0.010	He, 2017
Td1900-8	Phyllite				+0.15	0.05	0.24	116*10–4		0.002	
Td1900-3	Phyllite				+0.34	0.02	0.37	220*10–4		0.002	
TBDB-4	Sandstone				+0.62	0.01	0.04	90*10–4		0.000	
TBS16-1	Graywacke				+0.33	0.05	0.05	11*10–4		0.005	
HS-8	Dolostone				+0.28	0	0.10	26*10–4		0.004	
YM-3	Breccia				+0.53	0.02	0.14	36*10–4		0.004	

with detailed procedures as described by He et al. (2016) and Zhu et al. (2018).

During the isotope analyses, the mass discrimination effects were corrected by the combined sample-standard bracketing (SSB) (Zhu et al., 2002). $\delta^{66/64}$Zn value (relative to IRMM 3702) of sphalerite samples was calculated using the equation of $\delta^{66/64}Zn$ (‰) = ($\delta^{66/64}Zn_{sample}/\delta^{66/64}Zn_{IRMM\ 3702}$ − 1) × 1000. Average $\delta^{66/64}$Zn value obtained from repeated analyses of the standard NIST SRM 683 (-0.13 ± 0.03‰, n = 5) and internal standard IRMM 3702 (0.00 ± 0.03‰, n = 32). The measured values are consistent with their respective recommended values, i.e., NIST SRM 683 ($\delta^{66/64}$Zn = -0.12‰; Yang et al., 2018) and IRMM 3702 ($\delta^{66/64}$Zn = 0.00‰; Zhu et al., 2020). The Zn isotope compositions were reported relative to the international JMC Lyon Zn standard 3-0749L, i.e., $\delta^{66}Zn_{JMC} = \delta^{66}Zn_{IRMM3702} + 0.27$ (Wang et al., 2017). The internal standard NIST SRM 3108 and secondary standard JMC Cd (lot#74–075219 k) were used for the Cd isotope measurement. $\delta^{114/110}$Cd value (relative to NIST SRM 3108) of the sphalerite samples were calculated with the formula $\delta^{114/110}Cd$ (‰) = ($\delta^{114/110}Cd_{sample}/\delta^{114/110}Cd_{\ NIST\ SRM\ 3108}$ − 1) × 1000. Repeated analyses of NIST SRM 3108 and JMC Cd solution yielded an average $\delta^{114/110}Cd$ = 0.00 ± 0.05‰ (n = 36) and −1.65 ± 0.05‰ (n = 4), respectively, consistent with the recommended values for the standard NIST SRM 3108 (0.00‰; Zhang et al., 2016) and JMC Cd solution (-1.56 to −1.63‰; Zhang et al., 2016). Sphalerite $\delta^{114/110}$Cd value of our samples were expressed relative to the internal standard Spex Cd, i.e., $\delta^{114}Cd_{spex} = \delta^{114}Cd_{NIST\ SRM\ 3108}$ + 0.11 (Zhang et al., 2016).

4. Results

4.1. Sulfur isotopes of sulfides

δ^{34}S values of 7 pyrite and 15 sphalerite separates are summarized in Table 1 and shown in Fig. 5. All samples have a narrow δ^{34}S range of + 20.05 to + 23.48‰ (avg. + 22.11‰, n = 22; Table 1). Pyrite separates have δ^{34}S values (+22.14 to + 23.48‰, mean + 22.87‰; n = 7) slightly higher than sphalerite separates (+20.78 to + 23.21‰, mean + 21.75‰, n = 15; Table 1).

4.2. Zinc isotopes of sphalerite

Zinc isotope compositions of different types of sphalerite are given in Table 2 and plotted in Figs. 6–10. All sphalerite separates have relatively homogeneous $\delta^{66}Zn_{JMC}$ values from + 0.28 to + 0.55‰ (mean + 0.44‰, n = 12; Table 2), displaying a narrow range of $\delta^{66}Zn_{JMC}$ with respect to the mineral color or sample localities along stratigraphy (e.g., 1LY-4①, ②, LY-10①, ② and LY-24-4①, ②; Table 2).

4.3. Cadmium isotopes of sphalerite

Cadmium isotope values of sphalerite separates are listed in Table 2 and plotted in Figs. 6–11. The δ^{114}Cd values vary from −0.12 to + 0.39‰ (mean + 0.09‰, n = 15; Table 2), wider than the δ^{66}Zn range. The $\delta^{114}Cd_{spex}$ value of the upper orebody (1723 to 1770 m adit; −0.04 to + 0.39‰, mean + 0.14‰; Fig. 6) is higher than that of the lower orebody (1650 m adit; −0.12 to + 0.14‰, mean −0.02‰; Fig. 6). Meanwhile, the reddish-brown sphalerite has $\delta^{114}Cd_{spex}$ value (-0.04 to + 0.39‰, mean + 0.12‰, n = 8; Table 2) slightly higher than the yellowish-brown sphalerite (-0.12 to + 0.25‰, mean + 0.05‰, n = 7; Table 2).

5. Discussion

5.1. Source of sulfur

Sources of sulfur in a hydrothermal system can be determined from the total S isotope composition ($\delta^{34}S_{\sum S}$) of the ore-forming fluid

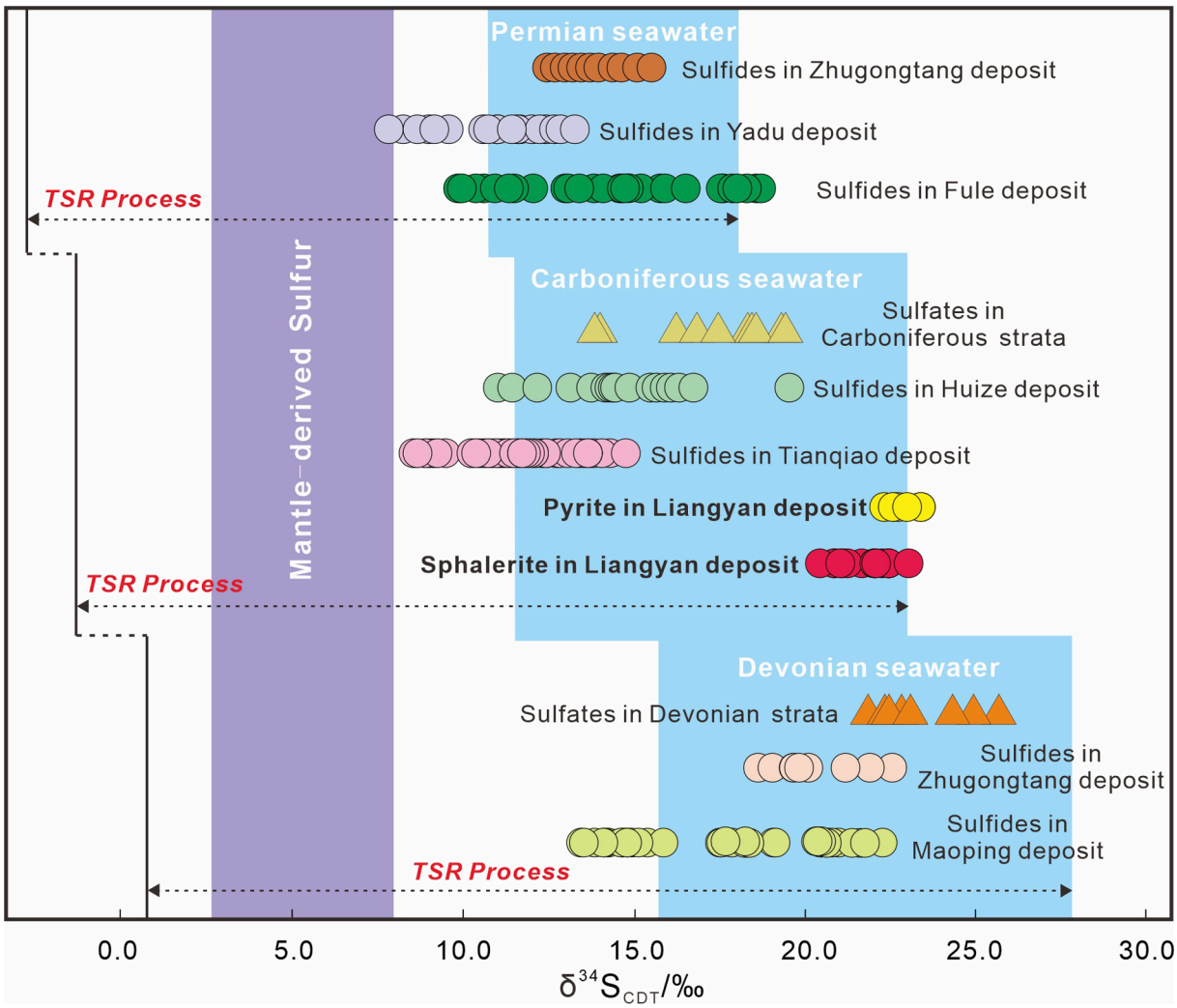

Fig. 5. Comparison of $\delta^{34}S$ value of sulfides, sulfates and seawater for the Zn-Pb deposits hosted in different strata in the SYGMP. Sulfur isotope data are from Zhou et al. (2013a, 2018), Ren et al. (2018), He et al. (2021), and Wei et al. (2021).

(Ohmoto and Rye, 1979). S-bearing minerals in the Liangyan deposit are dominantly sphalerite, galena and pyrite (Fig. 4 a-p), but sulfate minerals (e.g., barite and gypsum) are absent. Hence, the sulfur isotope compositions of sulfides can approximate that of the ore-fluid system (Ohmoto, 1972; Seal, 2006). Furthermore, pyrite separates have $\delta^{34}S$ values (+22.14 to + 23.48‰; avg. + 22.87‰) higher than those of the sphalerite separates (+20.78 to + 23.21‰; avg. + 21.75‰), suggesting thermodynamic equilibrium fractionation of S-isotope during the ore formation (Ohmoto, 1972; Zheng and Chen. 2000). Thus, the pyrite $\delta^{34}S$ value could approximate the ore-fluid $\delta^{34}S_{\sum S}$ value, i.e., $\delta^{34}S_{pyrite} \approx \delta^{34}S_{\sum S} \approx +22.87‰$.

The ore-forming temperatures of Zn-Pb deposits in the SYGMP are typical of 120 to 260℃, which are favorable for TSR (commonly > 100℃; Ohmoto and Rye, 1979) rather than BSR (optimal 60 to 80℃, maximum 110 ℃; Machel, 1989; Jørgenson et al., 1992). Thus, the reduced sulfur of most Zn-Pb deposits in the SYGMP was assumed to be provided by marine sulfates within the ore-hosting carbonates through the TSR process (Fig. 5), such as the Carboniferous host rocks for the Huize deposit (Li et al., 2006), Devonian host rocks for the Maoping deposit(He et al., 2020), Permian and Devonian host rocks for the Zhugongtang deposit (Wei et al., 2021), and Carboniferous host rocks for the Tianqiao deposit (Zhou et al., 2013a). However, some studies proposed that the reduced sulfur in some deposits in the SYGMP was sourced from multiple sulfur reservoirs, including the sulfates within the ore-hosting rocks and underlying sedimentary sequences with heavier sulfur isotopes (Fig. 5), such as those in the Fule Zn-Pb deposit (Zhou et al., 2018; Li et al., 2020).

Different from the mantle-derived sulfur reservoir (−5 to + 5‰; Ohmoto and Rye, 1979), the $\delta^{34}S$ values (+20.05 to + 23.48‰) of sulfides from the Liangyan deposit are similar to the Carboniferous seawater (+12 to + 22‰; Claypool et al., 1980) and the Carboniferous sulfates in the SYGMP (gypsum and barite: +13 to + 20‰; Ren et al., 2018). Relative to the theoretical $\delta^{34}S$ value (-2 to + 20‰, max $\Delta\delta^{34}S_{sulfate\text{-}sulfide} \approx +15‰$; Machel et al., 1995; Worden et al., 1995) generated by TSR of the Carboniferous marine sulfates, the measured $\delta^{34}S$ values of the Liangyan deposit are obviously higher. Such sulfide $\delta^{34}S$ values imply a possible input of S from heavier sulfur isotope source (s), rather than a single sulfur source (Ding et al., 2016; Wu et al., 2021a). Previous studies suggested that sulfates from the underlying Ediacaran to Devonian strata have $\delta^{34}S$ values ranging from + 22 to + 28‰ in the SYGMP (Zhou et al., 2013a; Ren et al., 2018; Wang et al., 2018). The theoretical TSR-generated $\delta^{34}S_{sulfide}$ values (+7 to + 28‰) of these sulfates overlap with the measured sulfide $\delta^{34}S$ values (+20.05 to + 23.48‰) of the Liangyan deposit, indicating that the sulfates within the Ediacaran to Devonian strata may be an additional sulfur source for the Liangyan deposit. We thus conclude that the reduced sulfur was most likely sourced from the mixing of multiple S reservoirs, i.e., sulfates in the Carboniferous ore-hosting strata and the Ediacaran to Devonian footwall.

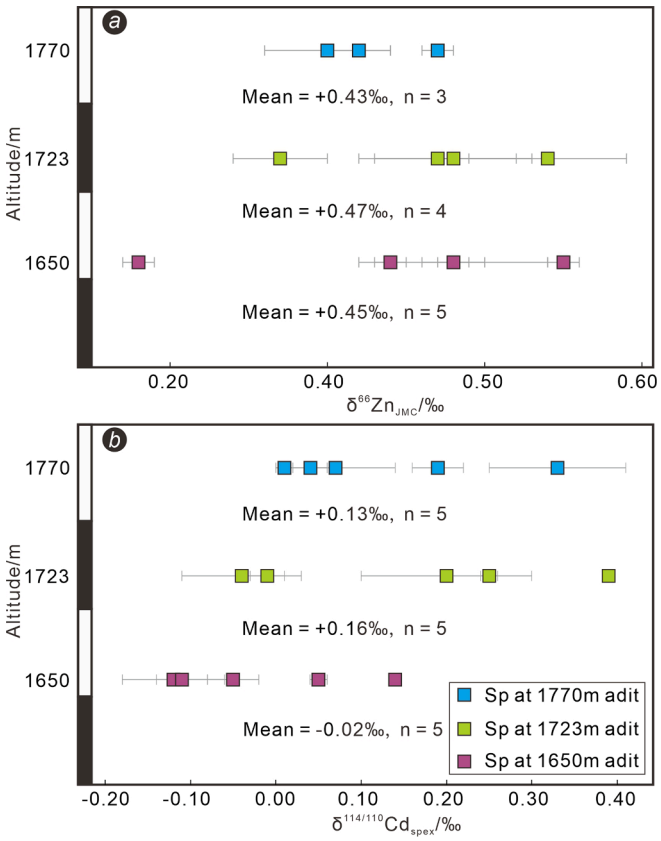

Fig. 6. $\delta^{66}Zn_{JMC}$ (a) and $\delta^{114}Cd_{spex}$ (b) values of sphalerite from different mine adits in the Liangyan deposit (field modified after Wu et al., 2021b).

5.2. Sources of metals

5.2.1. Possible source mechanism for Zn and Cd

Cadmium commonly enters the sphalerite lattice via substituting Zn^{2+}, due to their similar geochemical behavior (Schwartz, 2000; Cook et al., 2009; Wu et al., 2021b). The Zn and Cd isotopic fractionation between sulfides and hydrothermal fluids is limited, and thus the $\delta^{66}Zn$ and $\delta^{114}Cd$ values of sulfides could approximate those of the ore-forming fluids (Wombacher et al., 2003; Zhu et al., 2013; Xu et al., 2019; Zhang et al., 2019). In the Liangyan deposit, sphalerite separates with different color and stratigraphic variation have slightly different $\delta^{66}Zn_{JMC}$ value (+0.28 to + 0.55‰, avg. + 0.44‰; Table 2; Fig. 6a). The fractionation range between the reddish-brown (early-stage) and yellowish-brown (late-stage) sphalerite grains (e.g., 1LY-4①, ②, LY-10①, ② and LY-24-4①, ②) from the same ore sample is below 0.07‰ (Table 2). Such a narrow fractionation range is similar to sphalerite from the Maoping and Huize Zn-Pb deposits ($\delta^{66}Zn_{JMC}$ = +0.07 to + 0.25‰ and + 0.17 to + 0.55‰, respectively; Wu et al., 2021b; Wu, 2013), but is different from the sphalerite from the Banbanqiao ($\delta^{66}Zn_{JMC}$ = +0.07 to + 0.71‰) and Tianqiao ($\delta^{66}Zn_{JMC}$ = -0.26 to + 0.58) Zn-Pb deposits in the same ore province, where zinc isotopes were interpreted to be controlled by Rayleigh fractionation (Zhou et al., 2014a). Therefore, we consider that the narrow $\delta^{66}Zn_{JMC}$ range of sphalerite from the Liangyan deposit was mainly inherited from the mixing and homogenization of ore-forming fluids (Zhang et al., 2019; Wu et al., 2021b; Zhu et al., 2021), which is also supported by the above-mentioned narrow range of sulfide S isotopes.

Our samples have a wider range of $\delta^{114}Cd$ values (-0.12 to + 0.39‰, avg. + 0.09‰; Table 2) than that of $\delta^{66}Zn$ values. Sphalerite $\delta^{114}Cd_{spex}$ values of the ores from the upper orebody (-0.04 to + 0.39‰, avg. + 0.14‰; Fig. 6b) are higher than that of ores from the lower orebody (-0.12 to + 0.14‰, avg. −0.02‰; Fig. 6b), indicating that fluid mixing from different cadmium sources may have occurred. Although the reddish-brown sphalerite has slightly higher $\delta^{114}Cd_{spex}$ value (-0.04 to + 0.39‰, avg. + 0.12‰; Table 2) than the yellowish-brown sphalerite (-0.12 to + 0.25‰, avg. + 0.05‰; Table 2), there are three different $\delta^{114}Cd$ features for the dark and light-colored sphalerites from the same sulfide ore, namely (1) $\delta^{114}Cd_{dark\text{-}Sp}$ (LY-24-4②: +0.33‰) > $\delta^{114}Cd_{pale\text{-}Sp}$ (LY-24-4①: +0.19‰); (2) $\delta^{114}Cd_{dark\text{-}Sp}$ (LY-24-3②: +0.07‰) ≈ $\delta^{114}Cd_{pale\text{-}Sp}$ (LY-24-3①: +0.04‰); (3) $\delta^{114}Cd_{dark\text{-}Sp}$ (1LY-4①: −0.11‰) < $\delta^{114}Cd_{pale\text{-}Sp}$ (1LY-4②: −0.05‰). These features could not be reproduced by Rayleigh fractionation or temperature-controlled equilibrium fractionation (Wilkinson et al., 2005; John et al., 2008; Kelley et al., 2009; Yang et al., 2015).

It is reasonable to assume that isotope fractionation during the extraction of Zn and Cd from their potential source rocks was negligible, due to the similar geochemical behaviors of Zn and Cd (Metz and Trefry, 2000; Wilkinson et al., 2005; Zhu et al., 2021). Accordingly, ore-fluid mixing from two or more isotopically distinct sources could be a key factor for the Zn-Cd isotope variation of sphalerite from the Liangyan deposit. The different Zn and Cd isotopic variation ranges (narrow Zn and wide Cd isotopic range) may be caused by different proportions of input from their separate potential source rocks, i.e., the zinc and cadmium were possibly derived from different metal sources, as supported by negative correlations between $\delta^{66}Zn_{JMC}$ vs. $\delta^{114}Cd_{spex}$ (Fig. 7a) and $\delta^{66}Zn_{JMC}$ vs. $\delta^{34}S$ (Fig. 7b), and positive correlation between $\delta^{114}Cd_{spex}$ vs. $\delta^{34}S$ (Fig. 7c).

5.2.2. Source of Zn

Previous studies suggested the Neoproterozoic metamorphic basement, ore-hosting carbonate rocks and/or Permian Emeishan basalts to be the main potential metal sources in the SYGMP (Huang et al., 2004; Zhou et al., 2018; Zhu et al., 2021). The $\delta^{66}Zn_{JMC}$ values (+0.28 to + 0.55‰; Table 2) of sphalerite separates from the Liangyan deposit overlap with that of the basement rocks (+0.15 to + 0.62‰; Fig. 8; He, 2017) and Emeishan basalts (+0.25 to + 0.44‰; Fig. 8; Wu, 2013), and are generally higher than that of the Carboniferous carbonates (−0.12 to + 0.17‰; Fig. 8; He, 2017). The Cu-Ni-rich Emeishan basalts was considered unlikely to be a major Zn input for the Zn-Pb deposits in the SYGMP, owing to the major formation age gap (~50 Ma) between Emeishan basalts and Zn-Pb mineralization, the lower likelihood of leaching or extracting voluminous Zn-Pb from basalts, and the absence of Cu-Ni sulfide minerals (Zhou et al., 2002; Huang et al., 2004; Li et al., 2012; Yang et al., 2019; Xiang et al., 2020; Wu et al., 2021b). This is also supported by that the sulfide Pb isotope data of the Zn-Pb ores in NW Guizhou (e.g., Zhugongtang, Yadu, Shanshulin, and Tianqiao) fall in the field between the Devonian-Permian carbonate sequences and Neoproterozoic metamorphic basement, but distal from the Permian Emeishan basalts (Zhou et al., 2013a, 2014b, 2022; Wei et al., 2021; Wu et al., 2021b).

In the $\delta^{66}Zn_{JMC}$ vs. Cd/Zn plot (Fig. 9a), sphalerite separates from the Liangyan deposit fall along a negative linear trend (r = -0.55), suggesting that Zn was derived from binary fluid mixing between a high $\delta^{66}Zn$-low Cd/Zn and a low $\delta^{66}Zn$-high Cd/Zn end-member. As shown in Fig. 9a, the $\delta^{66}Zn_{JMC}$ values of sphalerite fall in the field close to the Neoproterozoic basement. Furthermore, high Zn content was reported in the basement rocks (avg. Zn content > 80 ppm; Table 2; He, 2017). We thus suggest that Zn was chiefly sourced from the Neoproterozoic basement, which contains high $\delta^{66}Zn$ and low Cd/Zn values. Besides, the Carboniferous carbonate wallrocks could be another possible Zn source. The wallrocks has relatively low $\delta^{66}Zn$ value but high Cd/Zn ratio, and the mixing of these two Zn sources (basement and wallrocks) could explain the negative linear trend between $\delta^{66}Zn_{JMC}$ vs. Cd/Zn (Fig. 9a). From the 1650 m (lower orebody) to 1770 m adit (upper orebody), the Zn/Cd ratios and $\delta^{66}Zn_{JMC}$ values of sphalerite gradually decrease (Fig. 10a), implying that the main ore-forming fluid may have shifted from the high-Zn high-$\delta^{66}Zn_{JMC}$ end-member (Neoproterozoic basement) to the lower-Zn low-$\delta^{66}Zn_{JMC}$ end-member (Carboniferous

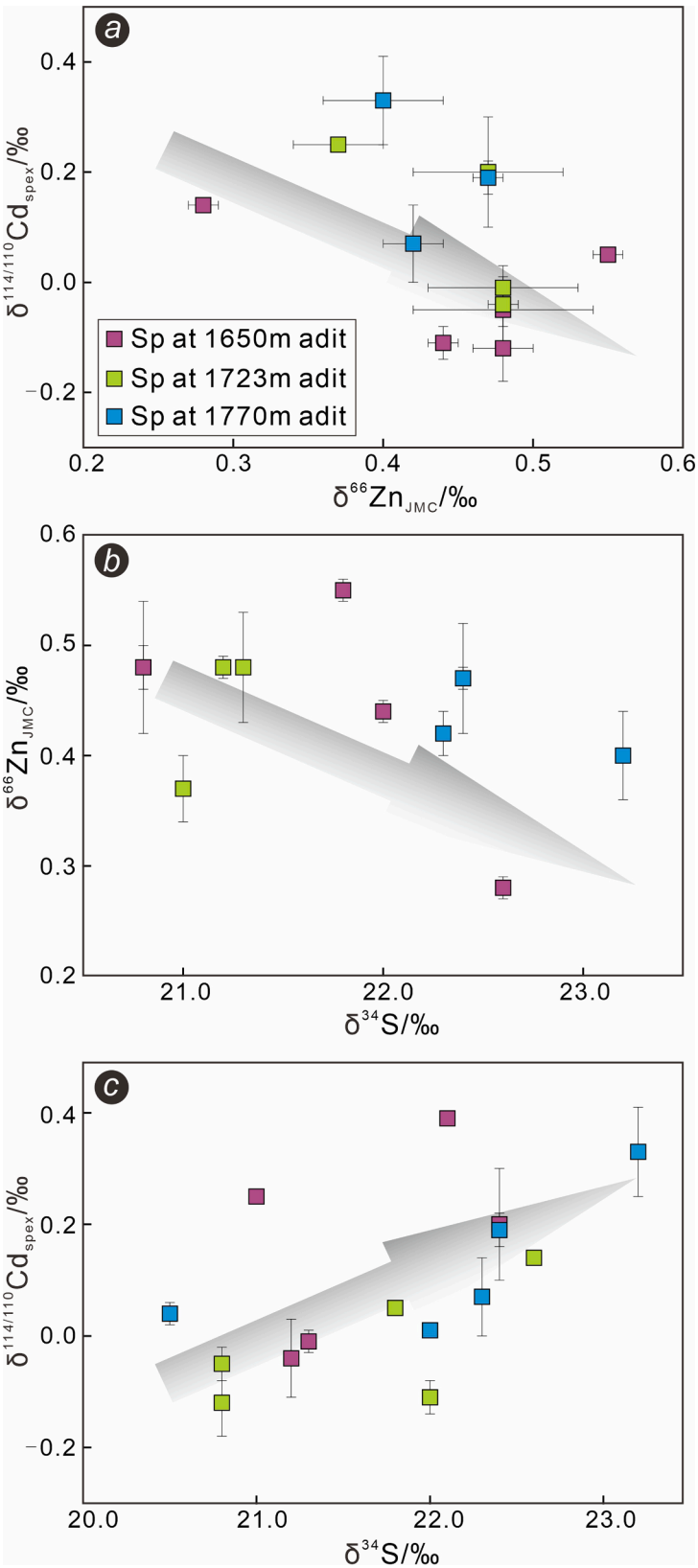

Fig. 7. Plots of $\delta^{114}Cd_{spex}$ vs. $\delta^{66}Zn_{JMC}$ (a), $\delta^{66}Zn_{JMC}$ vs. $\delta^{34}S$ (c) and $\delta^{114}Cd_{spex}$ vs. $\delta^{34}S$ (c) of sphalerite from different mine adits in the Liangyan deposit.

carbonates). Hence, we consider that Zn was mainly derived from the Neoproterozoic basement, and minor from the carbonate wallrocks. This is supported by Sr isotopes studies of sphalerite from some representative Zn-Pb deposits in NW Guizhou (incl. Tianqiao, Shanshulin, and Shaojiwan), which suggested that the Zn and Sr in sphalerite have likely an identical source, i.e., a mixed source that includes both the basement rocks and the Ediacaran-Permian sedimentary sequences (Dou et al., 2014; Zhou et al., 2013b, 2014b, 2022). A similar source mixing model

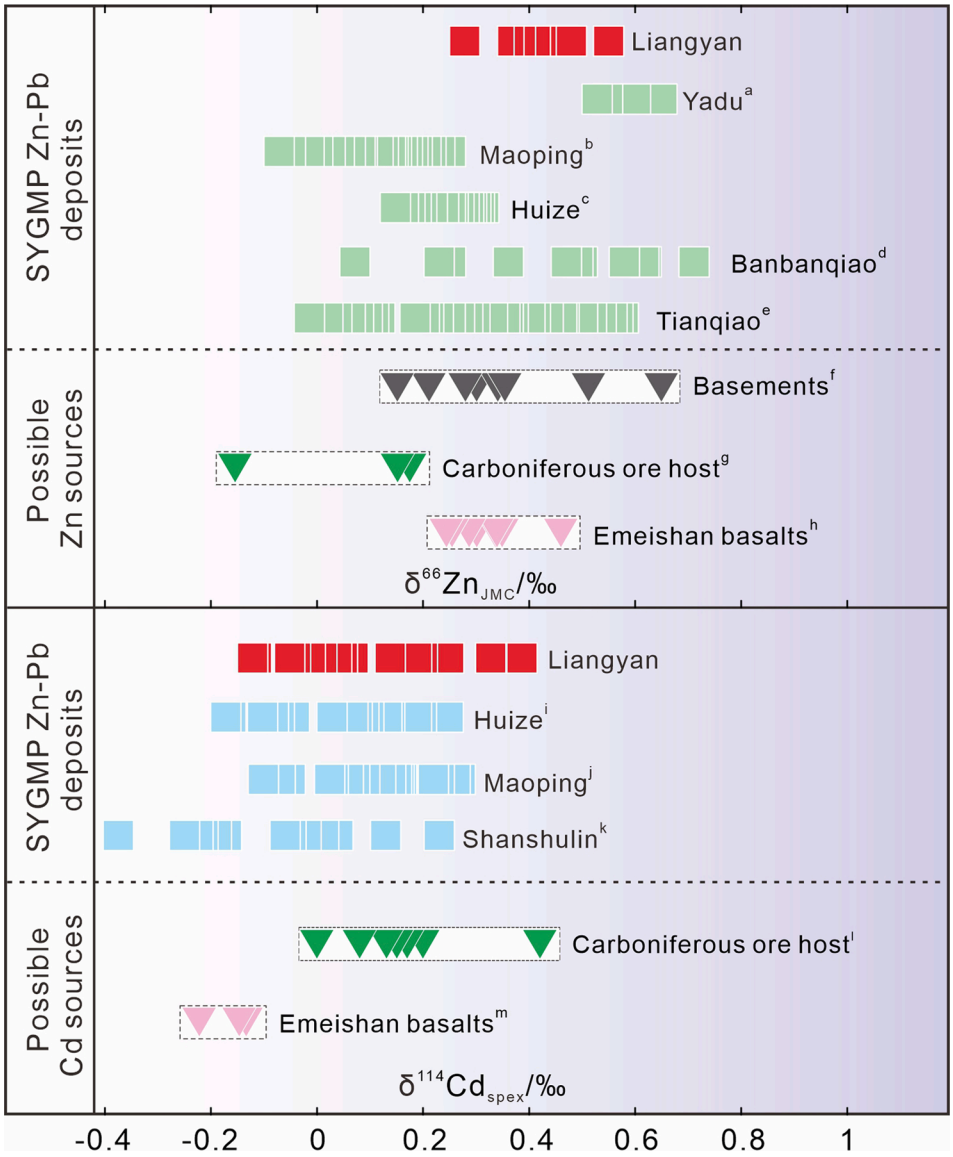

Fig. 8. Comparison of $\delta^{66}Zn_{JMC}$ and $\delta^{114}Cd_{spex}$ values between typical Zn-Pb deposits and possible source rocks in the SYGMP. Data source, a: He et al., 2021; b and j: Wu et al., 2021b; c and h: Wu, 2013; d and e: Zhou et al., 2014a; f and g: He, 2017, Zhou et al., 2014a; i, k and l: Zhu et al., 2021; m: Zhu et al., 2017.

for Pb and Zn were also proposed for some large Zn-Pb deposits (incl. Maoping, Zhugongtang, and Maozu) in the SYGMP, based on Pb and Zn isotope evidence of metallic sulfides (Xu et al., 2019; Wei et al., 2021; Wu et al., 2021b).

5.2.3. *Source of Cd*

A binary ore-fluid mixing model was proposed for Cd from many representative Zn-Pb deposits in the SYGMP, based on negative correlation of $\delta^{114}Cd_{spex}$ vs. Zn/Cd between the Devonian-Permian ore-hosting sedimentary rocks and the Emeishan basalts (Zhu et al., 2021). The $\delta^{114}Cd_{spex}$ values (−0.12 to + 0.39‰; Table 2) of sphalerite grains from the Liangyan deposit mostly overlap with that of the Carboniferous carbonate wallrocks (+0.08 to + 0.42‰; Fig. 8; He, 2017), and are generally higher than that of the Emeishan basalts (−0.22 to −0.13‰; Fig. 8; Zhu et al., 2021). Although $\delta^{114}Cd_{spex}$ data of basement rocks are lacking in the SYGMP, the terrestrial greywackes deposited in the basinal basement have commonly high $\delta^{114}Cd_{spex}$ value (+0.60 to + 2.00‰; Wombacher et al., 2003). Hence, considering the high $\delta^{114}Cd_{spex}$ and low Cd content (~0.1 ppm; Zhu, 2014; He, 2017), we suggested that the Neoproterozoic basement could not be a major Cd source.

We have summarized and compared the $\delta^{114}Cd_{spex}$ and Zn/Cd values of the Carboniferous carbonate rocks (Zhu et al., 2017, 2021), Emeishan basalts (Zhu et al., 2021) and sphalerite from the Huize (Zhu et al., 2021), Maoping (Wu et al., 2021b), Shanshulin (Zhu et al., 2017, 2021), and Liangyan carbonate-hosted Zn-Pb deposits (Fig. 9b). Almost all sphalerite data define a negative correlation trend (r = -0.58) between two endmembers, the high $\delta^{114}Cd_{spex}$–low Zn/Cd Carboniferous ore-hosting sedimentary rocks and the low $\delta^{114}Cd_{spex}$–high Zn/Cd Emeishan basalts, indicating isotopic mixing between the two (Fig. 9b). In the same diagram, sphalerite data plot mostly in the field of the Carboniferous sedimentary rocks, suggesting that Cd, like the reduced sulfur, was derived mainly from the Carboniferous wallrocks, as supported by the positive correlation between $^{114}Cd_{spex}$ and $\delta^{34}S$ (Fig. 7c) and the higher Cd content (avg. 0.49 ppm; Table 2) than the Emeishan basalts (avg. 0.15 ppm; Table 2) and basement rocks (avg. 0.13 ppm; Table 2). It is noteworthy that the Emeishan basalts may have also contributed some Cd, as the $\delta^{114}Cd_{spex}$ value of the lower orebody (proximal to the Emeishan basalts: −0.12 to + 0.14‰, avg. −0.02‰; Table 2) is lower than that of the upper orebody (distal from the Emeishan basalts: −0.04 to + 0.39‰, avg. + 0.14‰; Table 2). Moreover,

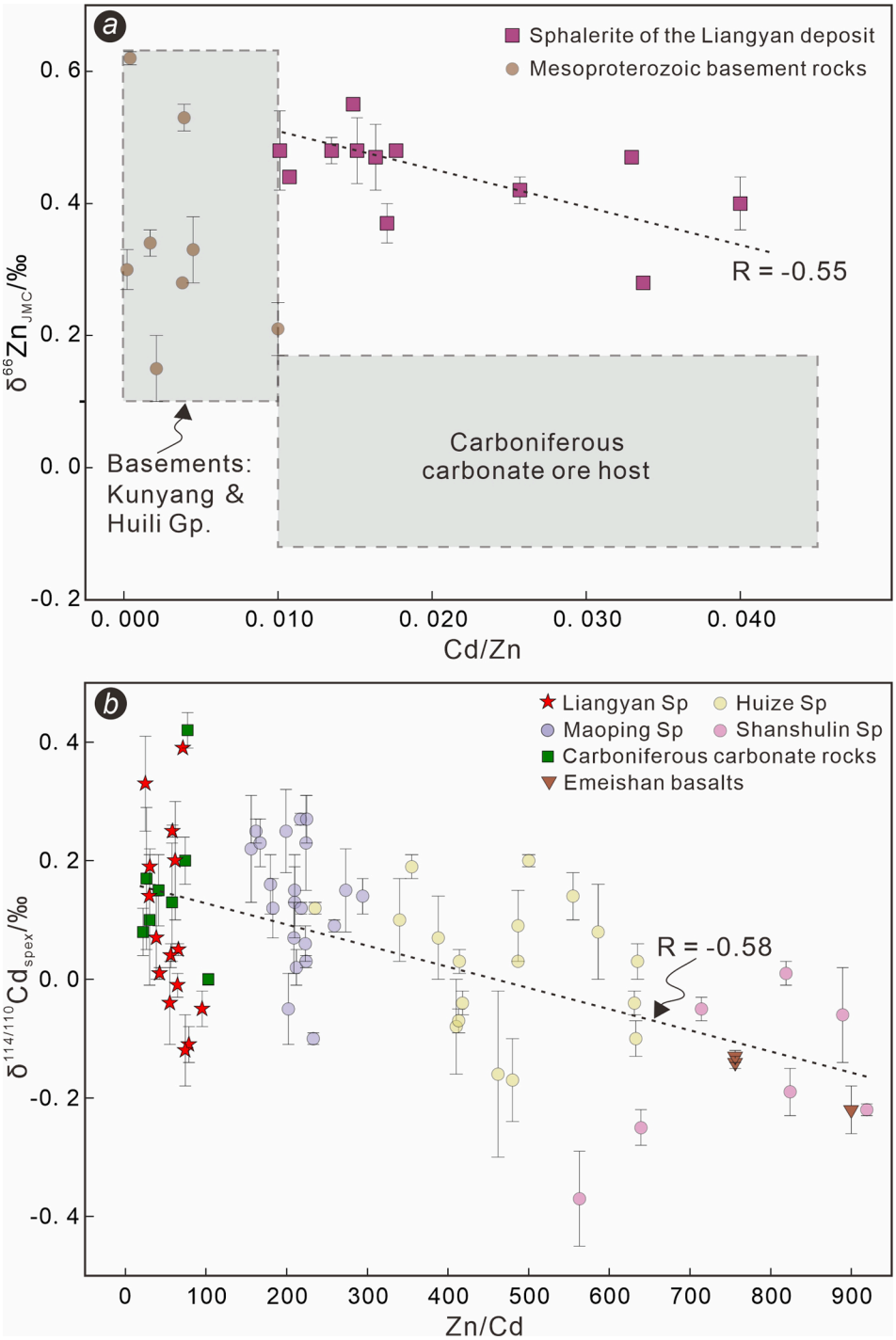

Fig. 9. (a) $\delta^{66}Zn_{JMC}$ vs. Cd/Zn plot of sphalerite from the Liangyan deposit, Mesoproterozoic basement rocks (He, 2017), and Carboniferous carbonate wallrocks (Zhu, 2014; He, 2017); (b) $\delta^{114}Cd_{spex}$ vs. Zn/Cd plot of sphalerite from the Liangyan and other typical Zn-Pb deposits in the SYGMP, Carboniferous carbonate wallrocks, and Permian Emeishan basalts (Zhu et al., 2017, 2021, Wu et al., 2021b).

the Cd/Zn and $\delta^{114}Cd_{spex}$ values of sphalerite gradually increase from the 1650 m to 1770 m adit (Fig. 10b), indicating that a Zn-rich basement-derived ore-fluid has successively leached Cd from the Emeishan basalts (with low Cd-$\delta^{114}Cd_{spex}$) and the Carboniferous carbonate rocks (with high Cd-$\delta^{114}Cd_{spex}$).

5.3. Implication for Zn-Pb mineralization at Liangyan

Cd isotopes and Zn/Cd ratios of sphalerite were used to identify high-temperature (magmatic hydrothermal, skarn, and VMS), low-temperature (MVT), and sedimentary exhalative Zn-Pb deposits (Wen et al., 2016; Xu et al., 2019). Sphalerite separates from the Liangyan deposit mostly have $\delta^{114}Cd_{spex}$ values (−0.12 to + 0.39‰) and Zn/Cd ratios (25.2 to 95.3) similar to MVT deposits. The Liangyan deposit is also simialr to typical MVT deposits in terms of geological and geochemical features (Table 3; Bradley and Leach, 2003; Leach et al., 2010). Thus, the Liangyan deposit can be best classified as an MVT deposit.

Sphalerite Rb-Sr dating indicates that Zn-Pb mineralization at Liangyan occurred in ~ 215 Ma (Wang et al., 2022) and is coeval with

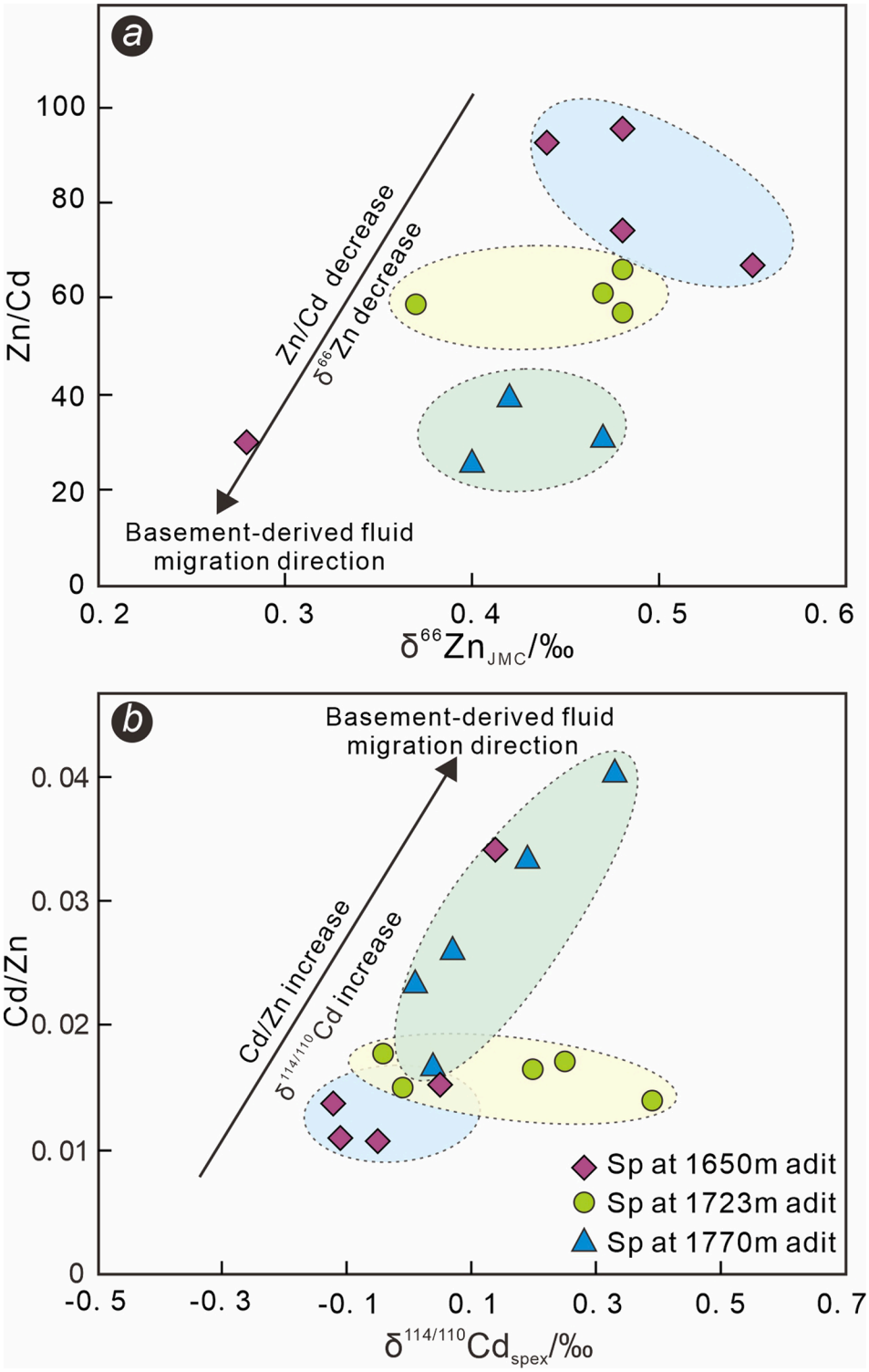

Fig. 10. $\delta^{66}Zn_{JMC}$ vs. Zn/Cd (a) and $\delta^{114}Cd_{spex}$ vs. Cd/Zn (b) plots of sphalerite from the Liangyan deposit.

the regional metallogeny induced by the Indosinian orogeny in the southwestern part of the Yangtze Block (Hu and Zhou, 2012; Zhang et al., 2015; Yang et al., 2019; Wu et al., 2021b; Han et al., 2022). The late Indosinian orogeny likely formed the Yadu-Wogong anticline and a series of NW-trending thrust faults, during the transition from the compression to extension (He et al., 2021; Han et al., 2022). Basement-derived metal-rich fluids (e.g., Zhong et al., 2015; Wei et al., 2021) ascended along the regional Yadu-Mangdong thrust fault (F_1) into the porous Carboniferous carbonate sequences. During the fluid migration, ore-forming elements were mobilized and leached from the wallrocks, such as Cd in the Emeishan basalts and carbonate wallrocks (as supported by Cd isotopes; Figs. 9 and 10b). Subsequently, this metal-rich fluid was trapped inside the Yadu-Wogong anticline and the secondary structures of the Yadu-Mangdong thrust fault (Figs. 2-3), providing an open-space for the mixing of basement-derived metal-rich fluid with preexisting reduced sulfur reservoirs, which were generated by TSR of marine sulfates from the Carboniferous sedimentary and Ediacaran-Devonian sequences. The fluid mixing may have caused rapid

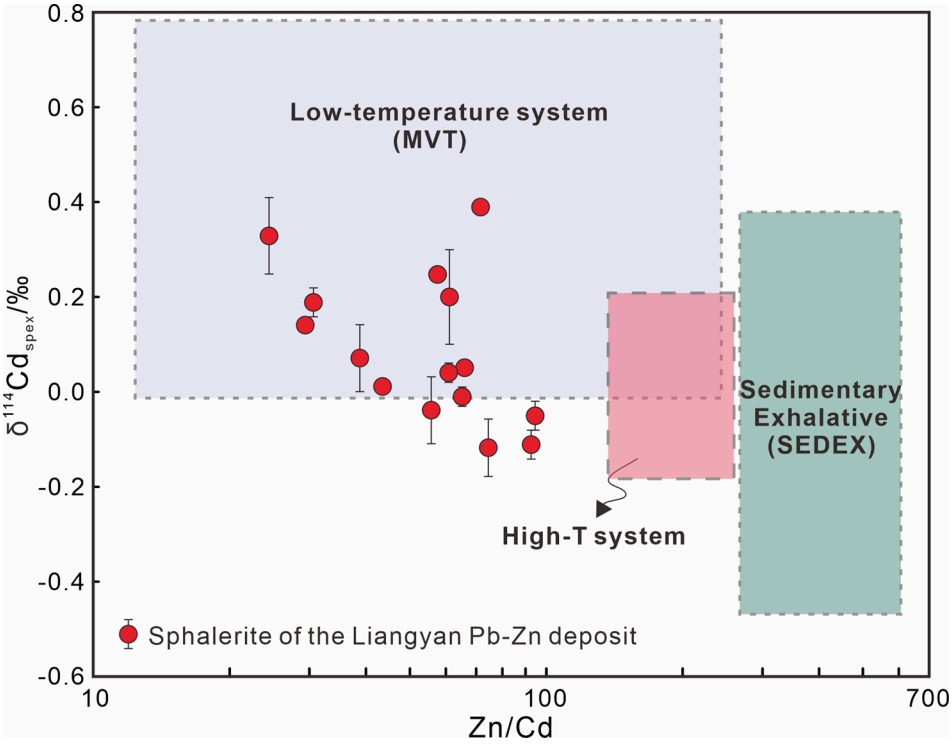

Fig. 11. Plot of $\delta^{114}Cd_{spex}$ vs. Zn/Cd for different mineralization systems (field modified after Wen et al., 2016).

Table 3
Geological comparison between the Liangyan deposit and typical MVT deposits.

Features	Liangyan Zn-Pb deposit	MVT Zn-Pb deposits
Ore-formation age	epigenetic, Early Jurassic (~215 Ma)	epigenetic, Proterozoic to Cretaceous
Tectonic background	thrust and fold belt	orogenic foreland basin, rifts in extensional environment, and thrust-fold belt
Relationship with magmatism	spatially associated with the Permian Emeishan basalts	no genetic link with igneous activity
Ore-hosting rocks	dolostone, limestone and bioclastic/dolomitic limestone	carbonate rocks
Ore-controlling structures	Yadu-Mangdong thrust fault and Yadu-Wogong anticline	fault, fold, and lithology
Orebody occurrences	stratiform, veined and lenticular	layered, stratoid, veined and lenticular
Ore textures	massive, disseminated, and veined	disseminated, massive, finegranular, brecciated, and colloidal
Ore minerals	sphalerite, galena, and pyrite	sphalerite, galena, pyrite, and marcasite
Gangue minerals	dolomite and calcite	dolomite, calcite, barite, fluorite, and quartz
Associated metals	Cd and Ag	Ag
Ore-forming fluid	low-temperature and low f_{O2} acidic reducing basinal brine	low-temperature and medium–high salinity basinal fluid
Sulfur source(s)	TSR of sulfates mainly from Carboniferous ore-hosting rocks and partially from Cambrian-Devonian sedimentary sequences	TSR or BSR of seawater sulfate
Metals source(s)	Zn mainly from basement rocks and Cd mainly from Carboniferous carbonates	Basement rocks
Precipitation mechanism	Mixing of reduced S and metals	Reduced S model, Sulfate reduction model, or Mixing of reduced S and metals
References	Liao et al., 2020; Wei et al., 2021; Wang et al., 2022; This study	Bradley and Leach, 2003; Leach et al., 2010

physicochemical change (e.g., temperature, pH), resulting in sulfide precipitation and increase in fluid acidity ($MCl(aq) + H_2S(aq) = MS(s) + H^+ + 4Cl^-$, where M is Zn, Pb, and Fe; Wei et al., 2021). The enhanced acidity of the ore-forming fluid may have promoted further dissolution of carbonate wallrocks, which provided more space for sulfide precipitation.

6. Conclusions

i. Sulfur of the Liangyan deposit was derived from thermochemical sulfate reduction (TSR) of sulfates from multiple S reservoirs, including mainly from the Carboniferous ore-hosting rocks and minor from the Ediacaran-Devonian sedimentary sequences.
ii. Both Zn and Cd have different sources. Zinc was likely mainly from the Neoproterozoic metamorphic basement and minor from the Carboniferous wallrocks, whereas Cd was mainly sourced from the Carboniferous carbonates with additional input from the Permian Emeishan basalts.
iii. The Liangyan deposit is best classified as a thrust-fault controlled MVT Zn-Pb deposit, and the mixing of different fluids was the trigger for the Zn-Pb mineralization.

CRediT authorship contribution statement

Tao Wu: Conceptualization, Methodology, Data curation, Writing – original draft, Data curation. **Yufan He:** Investigation, Resources, Writing – review & editing. **Zhiwei He:** Investigation, Resources, Writing – review & editing. **Zhilong Huang:** Funding acquisition, Project administration, Supervision, Validation. **Lin Ye:** Writing – review & editing. **Chen Wei:** Writing – review & editing. **Fan Haifeng:** Writing – review & editing, Methodology. **Yusi Hu:** Formal analysis, Data curation. **Lin Du:** Investigation. **Minshan Gun:** Investigation.

Declaration of Competing Interest

The authors declare that they have no known competing financial interests or personal relationships that could have appeared to influence the work reported in this paper.

Data availability

No data was used for the research described in the article.

Acknowledgments

This study was supported by the National Natural Science Foundation of China (92162218 and 42202099), the Guizhou Provincial Natural Science Foundation (ZK[2023]477), Major Collaborative Innovation Projects for Prospecting Breakthrough Strategic Action of Guizhou Province, China ([2022] ZD004), and China Postdoctoral Science Foundation (2021M703190). We are grateful to Editor-in-Chief Meifu Zhou, anonymous reviewers, and Prof. Zhilin Wang for their insightful comments.

References

Bradley, D.C., Leach, D.L., 2003. Tectonic controls of Mississippi Valley-type lead-zinc mineralization in orogenic forelands. Miner. Deposita 38, 652–667.

Claypool, G.E., Holser, W.T., Kaplan, I.R., Sakai, H., Zak, I., 1980. The age curves of sulfur and oxygen isotopes in marine sulfate and their mutual interpretation. Chem. Geol. 28, 199–260.

Cook, N.J., Ciobanu, C.L., Pring, A., Skinner, W., Danyushevsky, L., Shimizu, M., SainiEidukat, B., Melcher, F., 2009. Trace and minor elements in sphalerite: a LA-ICP-MS study. Geochim. Cosmochim. Acta 73, 4761–4791.

Ding, T., Ma, D.S., Lu, J.J., Zhang, R.Q., Zhang, S.T., 2016. S, Pb, and Sr isotope geochemistry and genesis of Pb-Zn mineralization in the Huangshaping polymetallic ore deposit of southern Hunan Province. China. Ore Geol. Rev. 77, 117–132.

Dou, S., Liu, J.S., Zhou, J.X., 2014. Strontium isotopic geochemistry of Tianqiao Pb-Zn deposit Southwest China. Chinese J. Geochem. 33, 131–137.

Han, R.S., Wu, P., Zhang, Y., Huang, Z.L., Wang, F., Jin, Z.G., Zhou, G.M., Shi, Z.L., Zhang, C.Q., 2022. New research progress in metallogenic theory for rich Zn-Pb-(Ag-Ge) deposits in the Sichuan-Yunnan-Guizhou triangle (SYGT) area, southwestern Tethys. Acta Geol. Sin. 96, 554–573.

He, Z.W., Li, Z.Q., Li, B., Chen, J., Xiang, Z.P., Wang, X.F., Du, L.J., Huang, Z.L., 2021. Ore genesis of the Yadu carbonate-hosted Pb-Zn deposit in Southwest China: Evidence from rare earth elements and C, O, S, Pb, and Zn isotopes. Ore Geol. Rev. 131, 104039.

He, Y.F., Wu, T., Huang, Z.L., Ye, L., Deng, P., Xiang, Z.Z., 2020. Genesis of the Maoping carbonate-hosted Pb-Zn deposit, northeastern Yunnan Province, China: evidences from geology and C-O-S-Pb isotopes. Acta Geochim. 39, 782–796.

He, C.Z., 2017. Zinc-Sulfur isotopic compositions of the Tianbaoshan carbonate hosted Pb-Zn deposit in Sichuan, China: implications for source of ore components. Master dissertation. Institute of Geochemistry, Chinese Academy of Sciences, Guiyang, pp. 1–65 (in Chinese with English abstract).

Hu, R.Z., Zhou, M.F., 2012. Multiple Mesozoic mineralization events in South China – An introduction to the thematic issue. Miner. Deposita 47, 579–588.

Hu, R.Z., Fu, S.L., Huang, Y.H., Zhou, M.F., Fu, S.H., Zhao, C.H., Wang, Y.J., Bi, X.W., Xiao, J.F., 2017. The giant South China Mesozoic low-temperature metallogenic domain: Reviews and a new geodynamic model. J. Asian Earth Sci. 137, 9–34.

Hu, Y.S., Wei, C., Ye, L., Huang, Z.L., Danyushevsky, L., Wang, H.Y., 2021. LA-ICP-MS sphalerite and galena trace element chemistry and mineralization-style fingerprinting for carbonate-hosted Pb-Zn deposits: Perspective from early Devonian Huodehong deposit in Yunnan. South China. Ore Geol. Rev. 136, 104253.

Hu, R.Z., Wen, H.J., Ye, L., Chen, W., Xia, Y., Fan, H.F., Huang, Y., Zhu, J.J., Fu, S.L., 2020. Metallogeny of critical metals in the Southwestern Yangtze Block. Chinese Sci. Bull. 65, 3700–3714 in Chinese with English abstract.

Huang, Z.L., Chen, J., Han, R.S., Li, W.B., Liu, C.Q., Zhang, Z.L., Ma, D.Y., Gao, D.R., Yang, H.L., 2004. Geochemistry and ore genesis of the Huize Giant Pb-Zn deposit in Yunnan Province, China: discussion on the relationship between the Emeishan flood basalts and Pb-Zn mineralization. Geological Publishing House, Beijing, pp. 1–214 (in Chinese).

Huang, Z.L., Hu, R.Z., Su, W.C., Wen, H.J., Liu, S., Fu, Y.Z., 2011. A study on the large-scale low-temperature metallogenic domain in southwestern China: significance, history and new progress. Acta Mineral. Sin. 31 (3), 309–314 in Chinese with English abstract.

John, S.G., Rouxel, O.J., Craddock, P.R., Engwall, A.M., Boyle, E.A., 2008. Zinc stable isotopes in seafloor hydrothermal vent fluids and chimneys. Earth Planet. Sci. Lett. 269, 17–28.

Jørgenson, B.B., Isaksen, M.F., Jannasch, H.W., 1992. Bacterial sulfate reduction above 100℃ in deep sea hydrothermal vent sediments. Science 258, 1756–1757.

Kelley, K.D., Wilkinson, J.J., Chapman, J.B., Crowther, H.L., Weiss, D.J., 2009. Zinc isotopes in sphalerite from base metal deposits in the Red Dog district, Northern Alaska. Econ. Geol. 104, 767–773.

Leach, D.L., Bradley, D.C., Huston, D., Pisarevsky, S.A., Taylor, R.D., Gardoll, S.J., 2010. Sediment-hosted lead-zinc deposits in earth history. Econ. Geol. 105, 593–625.

Li, B., Gu, X.C., Wen, S.M., Han, R.S., Sheng, R., Xu, G.R., Cao, Y., Wu, H., Zou, G.F., 2012. Effect of Emeishan basalt in northeast Yunnan on lead and zinc mineralization. Min. Resourc. Geol. 26, 95–100 in Chinese with English abstract.

Li, W.B., Huang, Z.L., Chen, J., Han, R.S., Zhang, Z.L., Xu, C., 2004. Rb-Sr dating of mineral assemblage from the Huize giant Zn-Pb deposit Yunnan Province. Acta Petrol. Sin. 24, 112–116 in Chinese with English abstract.

Li, X.B., Huang, Z.L., Li, W.B., Zhang, Z.L., Yan, Z.F., 2006. Sulfur isotopic compositions of the Huize super-large Pb-Zn deposit, Yunnan Province, China: implications for the source of sulfur in the ore-forming fluids. J. Geochem. Explor. 89, 227–230.

Li, Z.L., Ye, L., Hu, Y.S., Huang, Z.L., Wei, C., Wu, T., 2020. Origin of the Fule Pb-Zn deposit, Yunnan Province, SW China: insight from in situ S isotope analysis by NanoSIMS. Geol. Mag. 157, 394–404.

Liao, M., Su, P.Z., Li, P.B., Han, L., Kang, R.H., Li, Q.R., 2020. Verification report on resource reserves of the Liangyan-Wogong Pb-Zn deposit in Xingfa, Hezhang County, China. 418 Team of Hunan Geological and Mineral Bureau, pp. 1–100 (in Chinese).

Liu, H.C., Lin, W.D., 1999. Regularity research of lead-zinc-silver deposits in northeastern Yunnan Province. Kunming: Yunnan University Press, pp 1–468 (in Chinese).

Luo, K., Cugerone, A., Zhou, M.F., Zhou, J.X., Sun, G.T., Xu, J., He, K.J., Lu, M.D., 2022. Germanium enrichment in sphalerite with acicular and euhedral textures: an example from the Zhulingou carbonate–hosted Zn(–Ge) deposit, South China. Miner. Deposita doi.org/10.1007/s00126-022-01112-4.

Luo, K., Zhou, J.X., Huang, Z.L., Caulfield, J., Zhao, J.X., Feng, Y.X., Ouyang, H.G., 2020. New insights into the evolution of Mississippi Valley-Type hydrothermal system: a case study of the Wusihe Pb-Zn deposit, South China, using quartz in-situ trace elements and sulfides in situ S-Pb isotopes. Am. Mineral. 105, 35–51.

Luo, K., Zhou, J.X., Xu, C., He, K.J., Wang, Y.B., Sun, G.T., 2021. The characteristics of the extraordinary germanium enrichment in the Wusihe large-scale Ge-Pb-Zn deposit, Sichuan Province, China and its geological significance. Acta Petrol. Sin. 37, 2761–2777 in Chinese with English abstract.

Machel, H.G., 1989. Relationships between sulfate reduction and oxidation of organic compounds to carbonate diagenesis, hydrocarbon accumulations, salt domes, and metal sulfide deposits. Carbonate. Evaporite. 4, 137–151.

Machel, H.G., Krouse, H.R., Sassen, R., 1995. Products and distinguishing criteria of bacterial and thermo-chemical sulfate reduction. Appl. Geochem. 10, 373–389.

Ohmoto, H., 1972. Systematics of sulfur and carbon isotopes in hydrothermal ore deposits. Econ. Geol. 67, 551–579.

Ohmoto, H., Rye, R.O., 1979. Isotopes of sulfur and carbon. In: Barnes, H.L. (Ed.), Geochemistry of hydrothermal ore deposits, 2nd ed. John Wiley and Sons, New York, pp. 509–567.

Ren, S.L., Li, Y.H., Zeng, P.S., Qiu, W.L., Fan, C.F., Hu, G.Y., 2018. Effect of sulfate evaporate salt layer in mineralization of the Huize and Maoping lead-zinc deposits in Yunnan: evidence from sulfur isotope. Acta Geol. Sin. 92, 1041–1055 in Chinese with English abstract.

Seal, R.R., 2006. Sulfur isotope geochemistry of sulfide minerals. Rev. Mineral. Geochem. 61, 633–677.

Shu, L.W., Wang, B., Cawood, P.A., Santosh, M., Xu, Z.Q., 2015. Early Paleozoic and Early Mesozoic intraplate tectonic and magmatic events in the Cathaysia Block, South China. Tectonics 34, 1600–1621.

Wan, L.C., 2015. Mineralization-alteration spatiotemporal zoning and its prospecting application in the Hezhang Liangyan lead-zinc deposit, Northwestern Guizhou Province, China. Master dissertation. Kunming University of Science and Technology, Yunnan, pp. 1–110 (in Chinese with English abstract).

Wang, Y.J., Fan, W.M., Zhang, G.W., Zhang, Y.H., 2013. Phanerozoic tectonics of the South China Block: Key observations and controversies. Gondwana Res. 23, 1273–1305.

Wang, M.Z., Han, R.S., Zhou, W., Song, D.H., Luo, D., Zhou, J.F., Wu, R.L., 2019. Ore-forming structure analysis of the Liangyan lead-zinc mining area in northwestern Guizhou deposit concentration district. China. J. Geomech. 25 (2), 187–197 in Chinese with English abstract.

Wang, M.Z., Han, R.S., Zhou, W.H., Wu, S.C., Luo, D., Song, D.H., 2022. In situ geochemical and Rb-Sr dating analysis of sphalerite from the Liangyan Pb-Zn deposit in northwestern Guizhou, China: Implication for timing of ore formation. Ore Geol. Rev. 154, 105340.

Wang, L.J., Mi, M., Zhou, J.X., Luo, K., 2018. New constraints on the origin of the Maozu carbonate-hosted epigenetic Zn-Pb deposit in NE Yunnan Province. SW China. Ore Geol. Rev. 101, 578–594.

Wei, C., Huang, Z.L., Ye, L., Hu, Y.S., Santosh, M., Wu, T., He, L.L., Zhang, J.W., He, Z.W., Xiang, Z.Z., Chen, D., Zhu, C.W., Jin, Z.G., 2021. Genesis of carbonate-hosted Zn-Pb

deposits in the Late Indosinian thrust and fold systems: An example of the newly discovered giant Zhugongtang deposit. South China. J. Asian Earth Sci. 220, 104914.
Wen, H.J., Zhu, C.W., Zhang, Y.X., Cloquet, C., Fan, H.F., Fu, S.H., 2016. Zn/Cd ratios and cadmium isotope evidence for the classification of lead-zinc deposits. Sci. Rep. 6, 25273.
Wilkinson, J.J., Weiss, D.J., Mason, T.F.D., Coles, B.J., 2005. Zinc isotope variation in hydrothermal systems: Preliminary evidence from the Irish Midlands ore field. Econ. Geol. 100, 583–590.
Wombacher, F., Rehkämper, M., Mezger, K., Münker, C., 2003. Stable isotope compositions of cadmium in geological materials and meteorites determined by multiple-collector ICPMS. Geochim. Cosmochim. Acta 67, 4639–4654.
Worden, R.H., Smalley, P.C., Oxtoby, N.H., 1995. Gas souring by the thermochemical sulfate reduction at 140 °C. AAPG Bull. 79, 854–863.
Wu, T., Huang, Z.L., Ye, L., Wei, C., Chen, J., Yang, M., Yan, Z.F., Sui, Z.H., 2021a. Origin of the carbonate-hosted Danaopo Zn-Pb deposit in western Hunan Province, China: Geology and in-situ mineral S-Pb isotope constraints. Ore Geol. Rev. 129, 103941.
Wu, T., Huang, Z.L., He, Y.F., Yang, M., Fan, H.F., Wei, C., Ye, L., Hu, Y.S., Xiang, Z.Z., Lai, C.K., 2021b. Metal source and ore-forming process of the Maoping carbonate-hosted Pb-Zn deposit in Yunnan, SW China: Evidence from deposit geology and sphalerite Pb-Zn-Cd isotopes. Ore Geol. Rev. 135, 104214.
Wu, Y., 2013. The age and ore-forming process of MVT deposits in the boundary area of Sichuan–Yunnan–Guizhou provinces, Southwest China. Ph.D. dissertation. Chinese University of Geosciences, Beijing, pp. 12–151 (in Chinese with English abstract).
Xiang, Z.Z., Zhou, J.X., Luo, K., 2020. New insights into the multi-layer metallogenesis of carbonated-hosted epigenetic Pb-Zn deposits: A case study of the Maoping Pb-Zn deposit. South China. Ore Geol. Rev. 122, 103538.
Xu, C., Zhong, H., Hu, R.Z., Wen, H.J., Zhu, W.G., Bai, Z.J., Fan, H.F., Li, F.F., Zhou, T., 2019. Sources and ore-forming fluid pathways of carbonate-hosted Pb-Zn deposits in Southwest China: Implications of Pb-Zn-S-Cd isotopic compositions. Miner. Deposita 55, 491–513.
Yan, D.P., Zhou, M.F., Song, H.L., Wang, X.W., Malpas, J., 2003. Origin and tectonic significance of a Mesozoic multi-layer over-thrust system within the Yangtze Block (South China). Tectonophysics 361, 239–254.
Yang, Q., Liu, W., Zhang, J., Wang, J., Zhang, X., 2019. Formation of Pb-Zn deposits in the Sichuan-Yunnan-Guizhou triangle linked to the Youjiang foreland basin: evidence from Rb-Sr age and in situ sulfur isotope analysis of the Maoping Pb-Zn deposit in northeastern Yunnan Province, southeast China. Ore Geol. Rev. 107, 780–800.
Zhang, H.J., Fan, H.F., Xiao, C.Y., Wen, H.J., Zhu, X.K., Ye, L., Huang, Z.L., Zhou, J.X., 2019. Homogeneous Zn isotopic compositions in the Maozu Zn-Pb ore deposit in Yunnan Province, southwestern China. Ore Geol. Rev. 109, 1–10.
Zhang, C.Q., Wu, Y., Hou, L., Mao, J.W., 2015. Geodynamic setting of mineralization of Mississippi Valley-type deposits in world-class Sichuan–Yunnan–Guizhou Zn–Pb triangle, southwest China: implications from age-dating studies in the past decade and the Sm-Nd age of the Jinshachang deposit. J. Asian Earth Sci. 103, 103–114.
Zheng, Y.F., Chen, J.F., 2000. Stable Isotope Geochemistry. Sci. Press, Beijing, 1–316 (in Chinese).
Zhong, R., Brugger, J., Chen, Y., Li, W., 2015. Contrasting regimes of Cu, Zn and Pb transport in ore-forming hydrothermal fluids. Chem. Geol. 395, 154–164.
Zhou, J.X., Huang, Z.L., Zhou, M.F., Li, X.B., Jin, Z.G., 2013a. Constraints of C-O-S-Pb isotope compositions and Rb-Sr isotopic age on the origin of the Tianqiao carbonate hosted Pb-Zn deposit. SW China. Ore Geol. Rev. 53, 77–92.
Zhou, J.X., Huang, Z.L., Bao, G.P., 2013b. Geological and sulfur-lead-strontium isotopic studies of the Shaojiwan Pb-Zn deposit, southwest China: implications for the origin of hydrothermal fluids. J. Geochem. Explor. 128, 51–61.
Zhou, J.X., Huang, Z.L., Zhou, M.F., Zhu, X.K., Muchez, P., 2014a. Zinc, sulfur and lead isotopic variations in carbonate-hosted Pb-Zn sulfide deposits, southwest China. Ore Geol. Rev. 58, 41–54.
Zhou, J.X., Huang, Z.L., Lv, Z.C., Zhu, X.K., Gao, J.G., Mirnejad, H., 2014b. Geology, isotope geochemistry and ore genesis of the Shanshulin carbonate-hosted Pb-Zn deposit, southwest China. Ore Geol. Rev. 63, 209–225.
Zhou, J.X., Luo, K., Wang, X.C., Wilde, S.A., Wu, T., Huang, Z.L., Cui, Y.L., Zhao, J.X., 2018. Ore genesis of the Fule Pb-Zn deposit and its relationship with the Emeishan Large Igneous Province: evidence from mineralogy, bulk C-O-S and in situ S-Pb isotopes. Gondwana Res. 54, 161–179.
Zhou, M.F., Malpas, J., Song, X.Y., Robinson, P.T., Sun, M., Kennedy, A.K., Esher, C.M., Keays, R.R., 2002. A temporal link between the Emeishan large igneous province (SW China) and the end Guadalupian mass extinction. Earth Planet. Sci. Lett. 196, 113–122.
Zhou, Z.T., 2017. Spatiotemporal zoning and genesis of hydrothermal dolomite in the Hezhang Liangyan lead-zinc deposit, Northwestern Guizhou Province, China. Master dissertation. Kunming University of Science and Technology, Yunnan, pp. 1-94 (in Chinese with English abstract).
Zhu, C.W., 2014. Geochemistry of Cd and Ge, and their isotopes in Carbonate-hosted lead-zinc ore deposits in the boundary area of Sichuan, Yunnan and Guizhou Provinces. China. Ph.D. dissertation. Institute of Geochemistry, Chinese Academy of Sciences, Guiyang 1–123 in Chinese with English abstract.
Zhu, C.W., Wen, H.J., Zhang, Y.X., Fan, H.F., Fu, S.H., Xu, J., Qin, T.R., 2013. Characteristics of Cd isotopic compositions and their genetic significance in the lead-zinc deposits of SW China. Sci. China-Earth Sci. 56, 2056–2065.
Zhu, C.W., Wen, H.J., Zhang, Y.X., Fu, S.H., Fan, H.F., Cloquet, C., 2017. Cadmium isotope fractionation in the Fule Mississippi Valley-type deposit Southwest China. Miner. Deposita 52, 675–686.
Zhu, C.W., Wen, H.J., Zhang, Y.X., Huang, Z.L., Cloquet, C., Luais, B., Yang, T., 2021. Cadmium isotopic constraints on metal sources in the Huize Zn-Pb deposit SW China. Geosci. Front. 12, 101241.